Stability and Inter-domain Interactions Modulate Amyloid Binding Activity of a General Amyloid Interaction Motif

Eva Asp, Ming Proschitsky, Michal Lulu, Cassandra Rockwell-Postel, Haim Tsubery and Rajaraman Krishnan

Correspondence to Rajaraman Krishnan: *Proclara Biosciences, 85 Bolton Street, Suite 212, Cambridge, MA 02140, USA.*
Rkrishnan1972@gmail.com
https://doi.org/10.1016/j.jmb.2019.03.022
Edited by Ronald Wetzel

Abstract

The M13 tip protein, g3p, binds the C-terminal domain of the bacterial membrane protein TolA via β-sheet augmentation, facilitating viral entry into *Escherichia coli*. G3p binding leads to rearrangement of the β strands and partial unfolding of TolA. G3p also binds multiple amyloid assemblies with high affinity, and it can remodel them into amorphous aggregates. We previously showed that amyloid binding activity is defined by the two g3p N-terminal domains, which we call the general amyloid interaction motif (GAIM). GAIM–hIgG1Fc fusions, which add immune effector function to amyloid targeting of GAIM, mediate reduction of two CNS amyloid deposits, Aβ plaques and tau tangles, in transgenic animal models of neurodegenerative disease. We carried out site-directed mutagenesis of GAIM to identify variants with altered amyloid binding and remodeling activity. A small set of residues along the inner strands of the two domains regulates both activities. The specificity of amyloid binding is governed by individual domain stability and inter-domain interactions. Our studies reveal several lines of similarity between GAIM binding to amyloids and g3p binding to its *E. coli* membrane target, TolA. Based on these studies, we designed new GAIM fusions that show enhanced binding potency towards multiple amyloid aggregates.

Introduction

Recent advances in the understanding of structures of amyloid aggregates show that despite adopting similar cross-β sheet structures and sharing similar tinctorial properties such as binding Congo red and thioflavin T, the underlying structures show tremendous structural polymorphism with potential implications in disease progression [1,2]. For example, Aβ and tau amyloids that are major constituents of plaques and neurofibrillary tangles have been shown to consist of several different proteoforms of Aβ and phosphorylated tau, each adopting a unique conformation *in vivo* [3–6]. They partition between soluble forms and insoluble aggregates, cause distinct pathological phenotypes, and affect the progression of the disease [7–13]. Thus, ideal therapeutic agents must be able to bind several of these conformations to prevent cellular damage and spread of these aggregates.

We have previously shown that the minor capsid tip protein, g3p, from any of a group of closely related filamentous phages that target *Escherichia coli*, act as conformational binders broadly targeting multiple species of amyloid fibers. This activity is determined by the two N-terminal domains, N1 and N2, that comprise what we functionally refer to as the general amyloid interaction motif (GAIM) [14]. When fused to a human IgG1 Fc to create a GAIM dimer (Fig. 1a), GAIM–IgG1 fusions (GAIM fusions) are capable of binding and remodeling multiple species of amyloid fibers into amorphous aggregates [14]. Systemically administered GAIM fusions can mediate reductions of both Aβ and tau pathology in transgenic animal models [15], and GAIM fusions are currently in clinical trials for diseases involving protein misfolding (NCT03008161; NCT03610035). The molecular interactions involved in GAIM binding and fiber remodeling are only partially understood. Hydrogen–deuterium exchange NMR experiments with labeled Aβ42 fibers showed that GAIM engages discontinuous

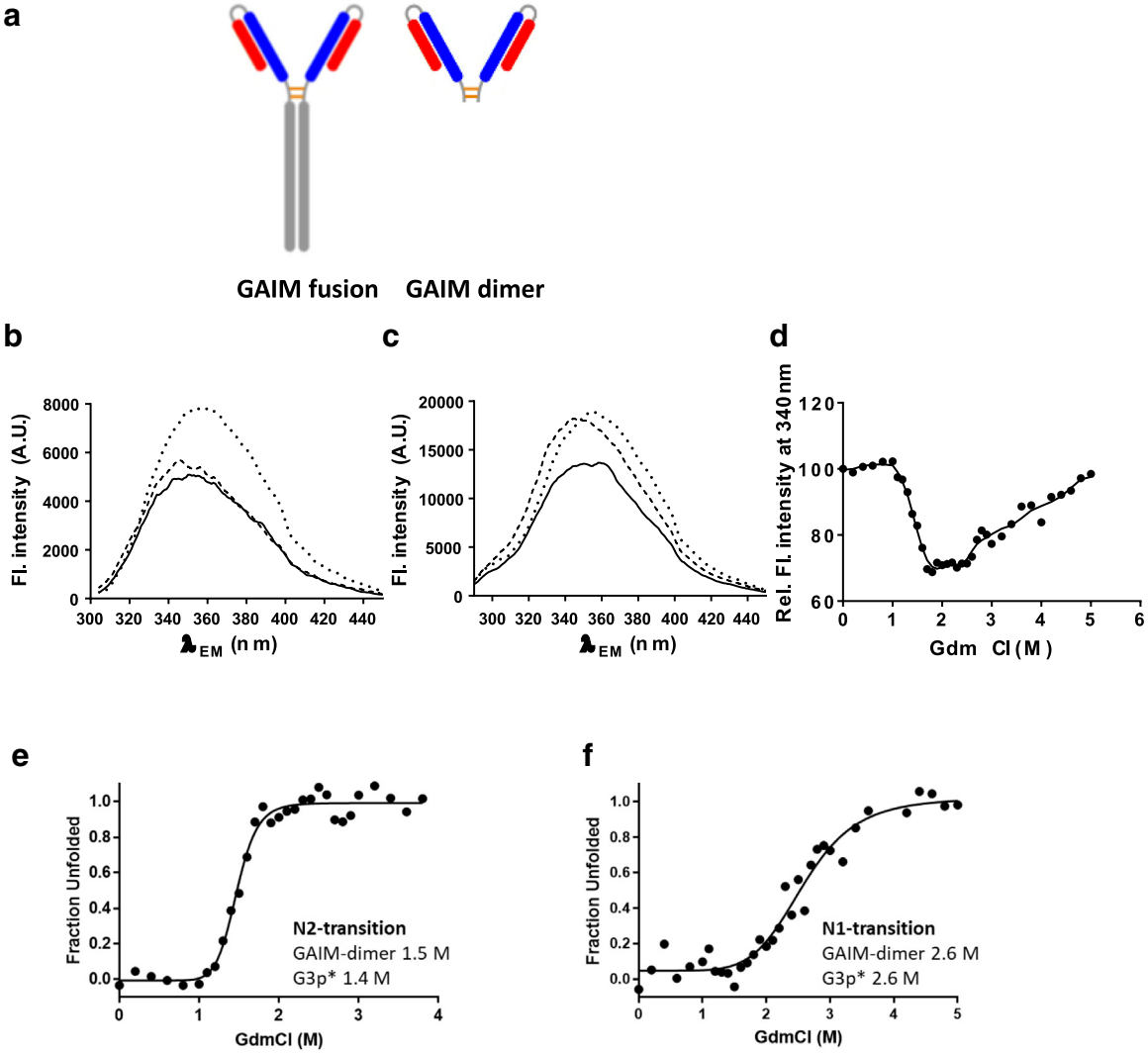

Fig. 1. Conformational properties of the GAIM dimer. (a) Schematic representation of the GAIM fusion and the cleaved GAIM dimer. The N2 and N1 domains are shown in blue and red, respectively, and the Fc domain and the hinge region with two disulfide bonds are shown in gray. (b) Fluorescence emission spectra of GAIM at 0 M (broken lines), 2 M (continuous lines), and 5 M GdmCl (dotted lines) excited at 295 nm and (c) 280 nm. (d) Relative fluorescence intensities at 340 nm (excitation 280 nm) with increasing concentration of GdmCl. Equilibrium unfolding of GAIM dimer in the presence of GdmCl shows two transitions, the first between 1 and 2 M GdmCl and the second between 2 and 4 M GdmCl. (e) Fractional changes of fluorescence at 310 nm (excitation 280 nm) and (f) 360 nm (excitation 295 nm) based on a two-state protein unfolding model. The N2 domain unfolds at 1.5 M GdmCl, and the denaturation transition of the more stable N1 domain takes place at 2.6 M GdmCl. *Previous reported denaturation transitions in g3p monomer are shown in comparison [17].

sequences on the fibril core and binds both sequences rich in aromatic residues (residues 17–25 in Aβ42) and aliphatic residues (31–40 in Aβ42). Furthermore, binding competitions with luminescent conjugated polythiophenes that intercalate along the amyloid fiber axis suggest that GAIM aligns along the fiber axis [14].

The two N-terminal domains of g3p, N1 and N2, adopt an inverted horseshoe conformation and are held together by an intricate network of hydrogen bonds [16] that determine the non-infectious closed state of the molecule. A *cis–trans* isomerization of the prolines in the inter-domain linker leads to progressive breakage of the hydrogen bonds and partial opening of the two domains. This rearrangement exposes the β strands 4 and 5 containing polar residues on N1, and β strands 9 and 10 containing aromatic residues on the N2 domain [16]. The opening of the inner central channel of the g3p horseshoe allows g3p to engage TolA and initiate viral infection. Mutations that stabilize the *cis* conformation of proline and/or introduce stabilizing hydrogen bonds reduce phage infection, while mutations that favor

the *trans* proline conformation and weaken hydrogen-bond stability leading to an open-state, increase infection [17,18].

We have previously shown that phage mutations that adopt a more open conformation and bind TolA-C also bind more potently to amyloid aggregates, while phage with closed g3p conformations bind amyloids poorly [14]. These observations led us to hypothesize that GAIM binding to amyloids is similar to g3p-TolA-C binding and might involve a similar interdomain unfolding and *cis–trans* isomerization of proline residues.

Here, we describe site-directed mutagenesis studies to probe the binding mechanism of GAIM domains to amyloid aggregates. Our results show that GAIM-amyloid binding potency correlates with the proportions of open or closed conformations of GAIM, and that minor changes along the inner surfaces of the horseshoe strongly influence binding potency, intra- and inter-domain stability, and non-specific binding. Taken together, we show that the structure–activity of phage attachment protein g3p is congruent with its structure–activity for amyloid binding. Using this information to create more potent amyloid targeting GAIM variants, we engineered a new class of open and stabilized GAIM fusions that bind Aβ and tau fibers with improved potency, inhibit their assembly, and more efficiently remodel them to amorphous conformers. The open structure of GAIM also allows these fusions to engage several sequentially and morphologically different misfolded amyloid conformers of Aβ, tau, bacterial CsgA, immunoglobulin light chains, and transthyretin (TTR). These studies further extend the mechanistic understanding of a novel class of therapeutic candidates based on the GAIM platform for targeting protein misfolding diseases.

Results

Structural features of GAIM are retained on the dimeric Ig-fusions

GAIM fusions display 2 copies of GAIM per molecule (Fig. 1a). To determine if the conformational state of the dimeric GAIM in the IgG fusion is similar to monomeric g3p, GAIM dimers were generated by a cysteine protease. This protease specifically cleaves the Fc fusion below the hinge, separating the Fc fragment from the two copies of GAIM linked by two disulfide bonds (Fig. 1a). After confirming the removal of Fc fragments by SDS-PAGE, protein unfolding studies were carried out on the resulting GAIM dimer.

The N1 and N2 domains of g3p have an asymmetric distribution of aromatic amino acids. The N2 domain contains 11 tyrosine (Y) residues and 1 tryptophan (W) residue that is solvent exposed in the closed state of g3p; the N1 domain contains 3 Y and 3 W residues. Thus, the intrinsic fluorescence of tyrosine and tryptophan residues allows for differential monitoring of conformational changes in N2 and N1 domains, respectively [19]. Guanidine hydrochloride (GdmCl) induced unfolding of the g3p monomer, followed by changes in intrinsic fluorescence, shows two major transitions [19]. The first transition (at 1.4 M GdmCl) represents the separation of the two domains, N1 and N2, and the simultaneous unfolding of the less stable N2 domain. The second transition (at 2.6 M GdmCl) represents the unfolding of the more stable N1 domain [19].

To follow unfolding of GAIM cleaved from the Ig fusion, GAIM dimers were equilibrated in 0, 2, and 5 M GdmCl solutions for 2 h at 25 °C. Selective excitation of the tryptophan residues at 295 nm showed a minimal change in GAIM dimer fluorescence intensities between 0 and 2 M GdmCl concentrations with no change in the emission λmax (345 nm) (Fig. 1b). At 5 M GdmCl, the tryptophan fluorescence was red-shifted by 15 nm (λmax 360 nm) and the fluorescence intensity was significantly higher than both 0 and 2 M samples. GAIM dimers were then excited at 280 nm (excitation of both W and Y residues) and the fluorescence emission spectra recorded (Fig. 1c). The fluorescence emission intensity at 340 nm decreased between 0 and 2 M GdmCl and then increased by a comparable margin at 5 M GdmCl. Similar spectral changes were also observed for monomeric g3p [19].

Next, we generated detailed denaturation profiles of GAIM dimers by recording fluorescence emission intensities at 310, 340, and 360 nm in a range of GdmCl concentrations. GAIM dimers show a biphasic denaturation profile at 340 nm when excited at 280 nm (Fig. 1d). The first transition occurs between 1 and 2 M GdmCl and the next between 2 and 4 M GdmCl. We then fitted the 310-nm (excitation 280 nm) and 360-nm (excitation 295 nm) denaturation profiles to a two-state protein unfolding model (Fig. 1e and f, respectively) and calculated the N2 and N1 domain denaturation transitions to be 1.5 and 2.6 M GdmCl, respectively. These results show that the N2 domains of GAIM unfold earlier than the N1 domains, as described for the g3p monomer, and GAIM domains in the dimer behave as two independently folded units, each with a conformation comparable to the monomeric g3p.

N1–N2 inter-domain interactions in GAIM fusions regulate amyloid fiber binding activity

To explore how GAIM mediates binding to amyloids, we carried out site-directed mutagenesis of β strands facing the inner groove of the GAIM domains, β strands 4 and 5 in the N1 domain and 9 and 10 in the N2 domain (Fig. 2a). These β strands facilitate inter-domain interactions in the closed state of g3p and prevent the premature exposure of the

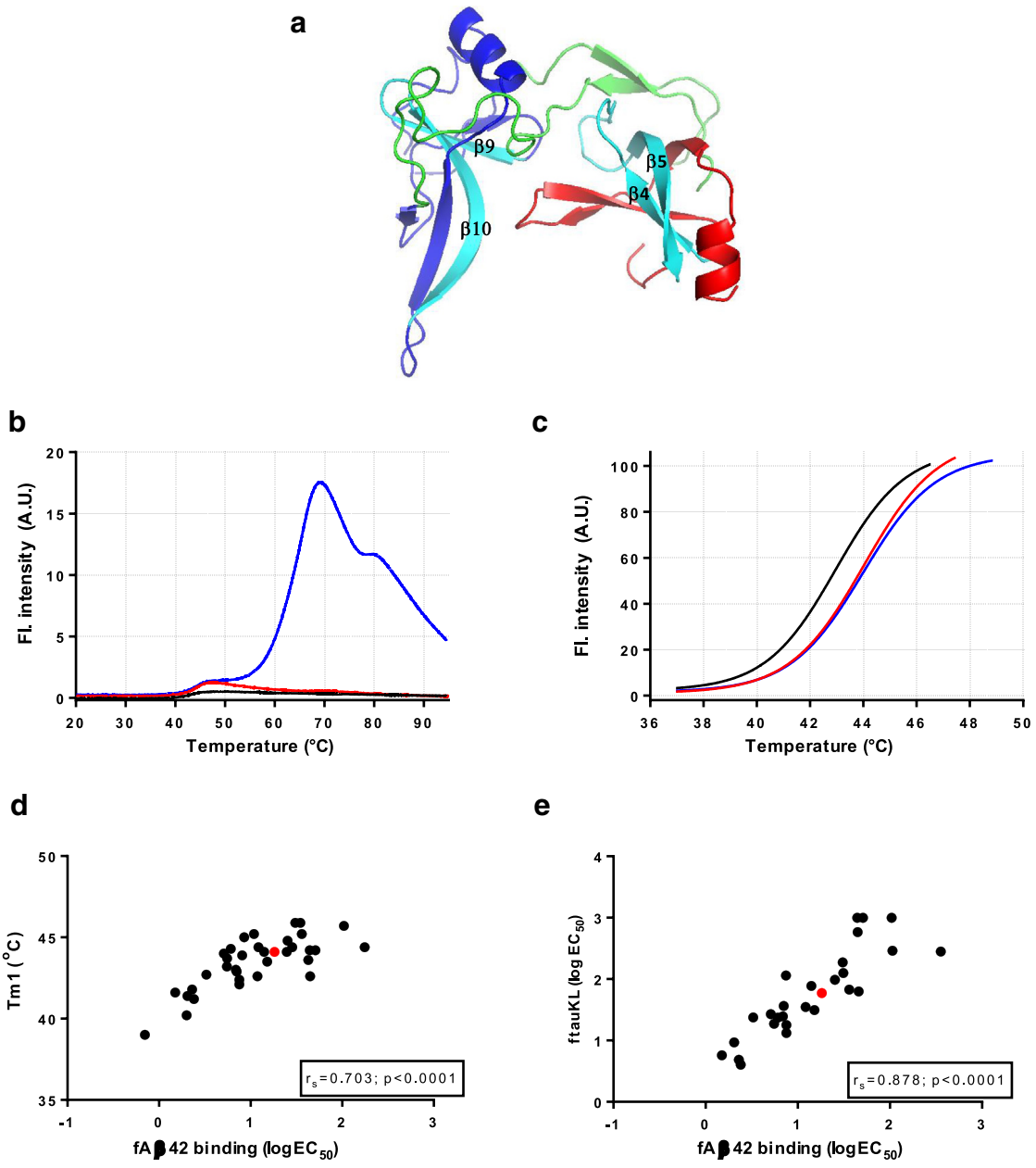

Fig. 2. Mapping residues modulating amyloid binding. (a) Tertiary structure of GAIM domains N1 (red) and N2 (blue) with the N2 hinge sub-domain (green). The b-strands subjected to site-directed mutagenesis marked in cyan (figure prepared by PyMolusing PDB structure 2G3P).(b) Thermal unfolding of GAIM monomer (black), GAIM dimer (red), and GAIM fusion (blue) followed by SO. (c) The first transition, Tm1, is calculated by non-linear fitting (four parameters) from normalized fluorescence intensities; GAIM monomer Tm1 = 43.0 °C, GAIM dimer Tm1 = 44.0 °C, and GAIM fusion Tm1 = 44.0 °C.(d) Aβ42 fiber binding activity of GAIM variants correlates with Tm1 (Spearman correlation coefficient = 0.703, $p < 0.0001$). A decrease in Tm1 represents a more open conformation of GAIM resulting in increased binding, and stabilized variants with higher Tm1 lose their binding activity. GAIM fusion scaffold NPT1098 is shown in red. (e) Changes in the binding potency of GAIM are tightly correlated for two different amyloids, fAb42 and ftauKL (Spearman correlation coefficient = 0.862, $p < 0.0001$). Variants with poor ftauKL binding are presented with an EC_{50} = 1000 nM due to inaccuracy in the curve fit for variants that does not reach saturation in the ELISA.

TolA-C binding site [20]. In addition, sites in the inter-domain hinge region involved in N1–N2 domain rearrangement from closed to open state during phage infection [16,21] were mutated to investigate how g3p activity during infection might translate to GAIM amyloid binding activity.

Prior to conducting the site-directed mutagenesis screen, several mutations were introduced in GAIM to potentially reduce immunogenicity. One predicted N-linked glycosylation site in the N1 domain, T41, was substituted with G to eliminate potential glycosylation. Potential T-cell epitopes in GAIM were removed through the following amino acid substitutions: K174R, V215A, and G220E (Supplementary Fig. 1). This molecule, NPT1098, binds to both Aβ1–42 fibers (fAβ42) and fibers assembled with tau-microtubule binding sequence with the P301L mutation (ftauKL) and was used as the scaffold for further mutagenesis studies.

The protein quality of the mutated GAIM fusion variants was assessed by size-exclusion chromatography (SEC) and SDS-PAGE and then screened for amyloid fiber binding activity to fAβ42 and ftauKL by ELISA. To compare binding activity and conformational stability of the GAIM fusion variants, a Sypro Orange (SO) binding assay was carried out [22]. SO binds poorly to the closed conformation of folded GAIM in an aqueous solution. When the two domains of GAIM dissociate and expose hydrophobic residues, the dye binds to the exposed hydrophobic surfaces and shows increased fluorescence. Thermal unfolding of the GAIM monomer expressed by *E. coli* and purified as described by Krishnan *et al.* [14] shows a single transition around 43 °C that corresponds to the domain opening and N2 unfolding transition (Fig. 2b). GAIM dimers obtained by removing the Fc fragment from the GAIM fusion show similar thermal melting to the monomer, shifted 1 °C to 44 °C (Fig. 2c). The GAIM fusions have three distinct transitions upon thermal unfolding (Fig. 2b). The first transition, Tm1, occurs at 44 °C as seen in the GAIM dimers and represents GAIM specific unfolding. Two additional transitions, at 64 °C and 81 °C, denote the unfolding transitions of the domains in the Fc [23]. In addition, the GAIM fusion variants were tested for off-target binding at high concentration (1.8 μM, 100-fold higher than scaffold EC_{50} for fAβ42) to a fibrillar, non-amyloid substrate, collagen.

Most of the mutations tested in N1 and N2 residues facing the inner groove of GAIM were found to affect Aβ42 fiber binding by ELISA (Fig. 2d). Binding activities of the mutated GAIM variants range from 0.7 to 175 nM (EC_{50}), representing more than a 250-fold change in binding affinity to fAβ42. There is a high positive correlation ($r_s = 0.703$; $p < 0.0001$) between binding potency (EC_{50}) and the first melting transition (Tm1). A decrease in Tm1 suggests a more open conformation of GAIM with increased binding potency, while stabilized variants with higher Tm1 tend to lose binding activity. This is suggestive of an amyloid fiber binding motif in GAIM being exposed when the inter-domain interactions are weakened; this interpretation is consistent with our previous data showing that GAIM binding is temperature dependent [14]. To discern whether the change in binding activity for fAβ42 translates to other unrelated amyloid fibers, a subset of the GAIM variants were tested by ELISA for binding to amyloid fibers formed from tauKL. Comparing GAIM variants' binding activities (EC_{50}) for fAβ42 and ftauKL shows that changes in binding activity of GAIM are correlated ($r_s = 0.878$; $p < 0.0001$) for the two different amyloids (Fig. 2e).

These results show that amyloid binding activity of GAIM correlates with the open/closed conformation of the N1 and N2 domains, and that minor changes in the β strands making up the inner core of GAIM affect binding potency and inter-domain stability. Specific mutations in T51 and T56 in β5 were found to have opposite effect on binding efficacy, and these residues contribute to ftauKL binding specificity (Table 1). Replacing T56 with histidine (H) increased fAβ42 binding 2.5-fold, with a modest increase in ftauKL activity. T51H or G substitutions had a minor effect on fAβ42 binding but showed a significant reduction in ftauKL binding potency. Several alanine replacements in the TolA-C binding region in N1 and in the N2 hinge region, designed to identify potential amyloid binding sites in GAIM, resulted in low protein yields and reduced protein quality, based on SEC (Supplementary Table 1). These variants exhibited a decrease in Tm1 or had no detectable change in Sypro binding during thermal unfolding, suggesting that the inter-domain interactions are perturbed in GAIM and/or that the N2 domain is misfolded. In addition, these variants showed increased off-target binding to collagen. Thermal denaturation of the N2 domain in isolation shows the midpoint of thermal unfolding transition around 35 °C [18]. The N2 domain in isolation is also aggregation-prone and remains stable only when it is co-assembled in the presence of hinge and N1 domain (by about 10,000-fold) [16]. Taken together, these results suggest that poor protein quality and increased non-specific binding of GAIM could be driven by the inherent instability of the N2 domain when separated from the N1 domain [18]. This led us to investigate structural features of the N2 domain and determine ways of stabilizing this domain by mutagenesis.

N2 domain stability determines amyloid binding activity and specificity

The g3p N2 domain consists of three distinct structural elements: a globular section resembling

Table 1. Polar residues in β5 strand modulate tau amyloid binding.

Variant	Amino acid replacement	Tm1 (°C)	Faβ42 EC_{50} (nM)	FtauKL EC_{50} (nM)
NPT1098	–	44.1	18.0	59.0
NPT189	T56H	42.9	7.0	34.0
NPT1005	T51H	44.2	44.1	>9000
NPT1011	T51G	42.6	44.0	572.0

N1 in structure [24], an α-helix that forms the pilus binding site, and a hinge region that forms an extensive network of hydrogen bonds with the N1 domain. This hinge region also contains several proline residues, one of which, P213, has been implicated in initiating phage infection by maintaining g3p in an open, TolA-C binding-competent state. Previous mutagenesis studies on g3p aimed at understanding the mechanism of phage infection have identified several stable mutations in the N2 domain that accelerate folding and stabilize the inter-domain interactions of g3p [19,25]. We incorporated a number of these mutations to investigate how altered phage infectivity and increased N2 stability impact amyloid binding activities.

Several mutations in GAIM that stabilized the N2 domains decreased amyloid binding (Fig. 3a). Elimination of a proline containing loop in N2, accomplished by substituting residues 157–163 with QGGK (NPT1009), increased Tm1 by 3.6 °C and led to a 18-fold loss in fAβ42 binding (Fig. 3b). Likewise, amino acid replacements in two turns in N2, residues 136–139 to FQGN (NPT1020) and residues 144–147 to VNGV (NPT1021), stabilized N2 (Tm1) by 1.8 °C and 2.5 °C, respectively. As predicted, both variants show a reduced fAβ42 binding activity compared to the parent GAIM scaffold, NPT1098. Similarly, introducing the Q129H mutation (NPT1015), a stabilizing mutation in N2 [17] increased Tm1 by 2.3 °C and decreased fiber binding.

Next, we asked if the stabilizing N2 mutations could compensate for the decreased stability accompanying GAIM variants that adopt an active, open conformation, based on Tm1.

To create a more open conformation of GAIM, the 23–28 loop in N1, important for inter-domain interactions in g3p [16,26], was replaced with the homologous sequence EGDS from the filamentous phage IF1 and tested in combination with N2-stabilizing mutations. Both N1 and N2 domains are stable in the IF1g3p, which lacks stabilizing inter-domain interactions and adopts an open conformation, constitutively exposing the TolA-C binding site [27]. The presumed open and N2-stabilized GAIM variants were tested for amyloid binding and were found to display improved fiber binding activity (Fig. 3c) with $EC_{50} < 1.5$ nM, consistent with a more exposed and accessible amyloid fiber binding site. One exception is a variant combining all three N2-stabilizing mutations, with Tm1 = 52.7 °C, which resulted in a loss of fAβ42 binding activity (Fig. 3c). This could be due to major structural changes in N2 masking the amyloid interaction site(s) in GAIM, either by introducing intra-domain interactions or by over-stabilizing the N2 domain. The open-stabilized variants show no correlation between Tm1 and fAβ42 binding, suggesting an uncoupling of amyloid binding and N2-stability in these variants. All EGDS- and N2-stabilized variants display high protein quality by SDS-PAGE and chromatograph as monomers by SEC. In addition, there is a shift to shorter retention time by SEC, which is consistent with a more open GAIM conformer molecule occupying a larger volume (Supplementary Fig. 2b).

Open-stabilized GAIM fusions show increased TolA-C binding

The TolA-C binding site in the N1 domain is shielded in the fully folded g3p and is exposed only after F-pili binding, which initiates the structural rearrangement of g3p, breakage of intra-domain hydrogen bonds, and prolyl-isomerization in the hinge region. To further characterize the open-stabilized GAIM, two variants with T56H and the EGDS-loop substitution in N1 and FQGN stabilization of N2, NPT1079 and NPT1087, were tested for TolA-C binding by ELISA (Fig. 3d). NPT1087 has one additional amino acid replacement in N2, N143A, that further stabilizes the N2. Replacing threonine 56 in β strand 5 with a histidine (NPT189) in the NPT1098 scaffold had significant impact on TolA-C binding, EC_{50} = 130 pM, compared to the NPT1098 scaffold, EC_{50} = 74 nM. This could be due to a more open conformation of GAIM in NPT189 (lower Tm1 by 1.2 °C) and/or site-specific increase in binding affinity to TolA-C. The open-stabilized variants NPT1079 and NPT1087 show an additional increase in binding (EC_{50} = 50 pM), as predicted of a more open GAIM conformation. In-solution binding of g3p variants to TolA-C AEDANS showed a >70-fold increase in binding of the isolated g3p N1 domain with an exposed TolA-C binding site compared to the GAIM monomer [20]. The TolA-C binding potency reported here is significantly higher than previously reported for g3p monomer or g3pN1, likely due both to GAIM dimerization and to several additional amino acid substitutions in the N1 domain that favor an exposed TolA-C binding site.

Altered amyloid binding correlates with remodeling activity

We had previously shown that prolonged incubation of amyloid fibers with phage M13 or GAIM fusions alters the fiber morphology. These altered protein complexes show reduced thioflavin T (ThT) fluorescence and fail to adhere to negatively charged cellulose acetate membranes, which we attributed to conformational conversion of fibers to amorphous aggregates [14]. Formation of this altered species was dependent on both the concentration of the GAIM fusion added and the length of time the complex was incubated [14]. Here we study remodeling of amyloid fibers in greater detail and

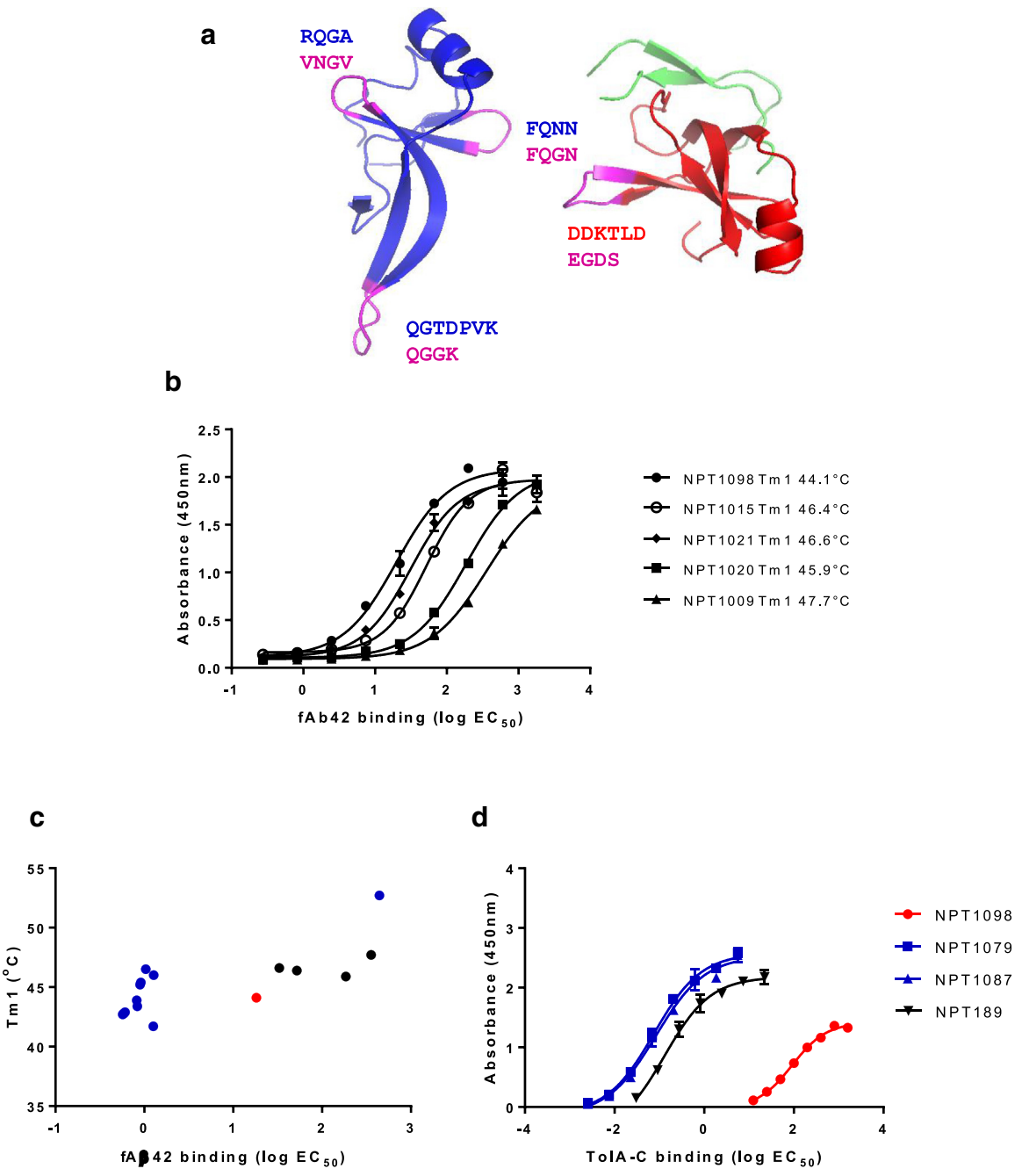

Fig. 3. Stabilizing N2 domain creating open-stabilized GAIM fusions. (a) The loop and turn stabilizing mutations in the N2 domain (blue) and the EGDS loop substitution in N1 domain (red) are shown in magenta. The two domains were prepared by PyMolusing PDB structure 2G3P. (b) Stabilizing mutations in the N2 domain reduces fAb42 binding by ELISA; NPT1015 (Q129H), NPT1021 (VNGV), NPT1020 (FQGN), and NPT1009 (QGGK).(c) Open-stabilized variants (blue) show increased fAb42 binding independent of their Tm1 with one exception, a super-stabilized N2 variant, Tm1 = 52.7 °C. (d) Introducing the T56H (NPT189) has significant impact on TolA-C binding, EC_{50} = 130 pM, compared to the scaffold NPT1098, EC_{50} = 74 nM. Additional mutations in the open-stabilized variants NPT1079 and NPT1087, EC_{50} ~ 50 pM, further increase the TolA-C binding.

characterize amyloid–GAIM fusion complexes using TEM imaging and solubility assays.

Figure 4a and b shows TEM images of Aβ42 fibers incubated with sub-stoichiometric GAIM fusion (Aβ42: NPT1098::25:1). When exposed to GAIM fusions, Aβ42 fibers lose their fibrillar architecture as seen in most of the uranyl acetate-stained samples. To establish that this alteration of structure reflected

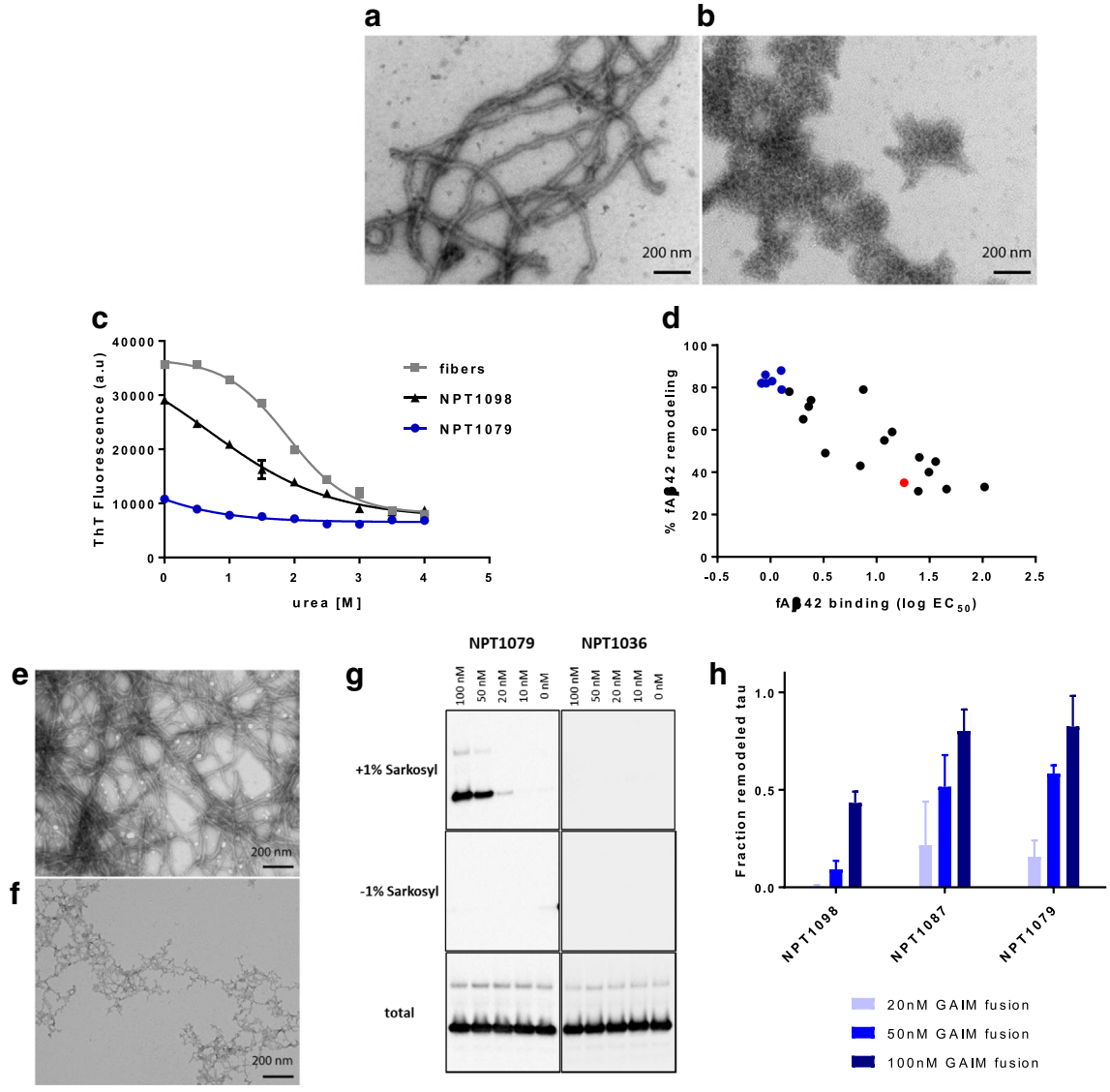

Fig. 4. GAIM–Ig fusions potently remodel amyloid aggregates. TEM images showing Aβ42 fibers before (a) and (b) after incubation with 0.8 mM NPT1079 at 37 °C for 6 days. (c) NPT1079-treated fAβ42 shown in panel b readily dissolves in urea. For comparison, ThT fluorescence of NPT1098-treated fibers and fibers alone in different concentrations of urea were plotted. (d) Remodeling activity of GAIM variants correlates with Aβ42 fiber binding affinities. Remodeling efficiency was calculated as loss in fiber-ThT fluorescence when compared to fibers alone at 1 M Urea. Open-stabilized variants (blue) show increased fAβ42 remodeling, and the GAIM scaffold NPT1098 (red) is shown in comparison. TEM images of tauKL fibers incubated without (e) and with (f) 100 nM NPT1079, at 37 °C for 3 days. (g) Sarkosyl solubility assay showing the presence of remodeled tauKL (monomers and dimers) in aggregates treated with NPT1079 (upper panel). NPT1036, a super-stabilized, disulfide-free GAIM with reduced infectivity (Kather *et al.*, [63]) with no binding activity to amyloid, did not show tau fiber remodeling. (h) Fraction remodeled tau (released tau in the 1% sarkosyl-fraction/total tau) is calculated from the total signal in each lane from the Western blot quantified by Image Lab (ChemiDocSystem BioRad). Error bars represents SD from three independent experiments.

remodeling of the fibers rather than non-specific GAIM binding and masking of fibrillar structures, we subjected the complexes and fibers to urea-induced denaturation. Aβ42 fibers are resistant to denaturation in low concentrations of urea, and less than 10% structural change is detected in 1 M urea, as measured by ThT fluorescence (Fig. 4c). ThT fluorescence drops dramatically in higher urea concentrations (2 M and above), suggesting loss of fibrillar structure. In contrast, fibers treated with

sub-stoichiometric amounts of different GAIM fusions begin to show 30%–90% reduced ThT binding at 1 M urea, suggesting that the fusions bind and alter fibrillar structures to a non-fibrillar state unable to bind ThT.

Next, we selected GAIM fusions with different Aβ42 fiber binding potencies and asked if the remodeling efficiencies correlate with the binding potencies and open conformational state. Figure 4d shows remodeling efficiencies of different GAIM fusions incubated with Aβ42 fibers under identical conditions and concentrations. Open-stabilized variants with low-nanomolar fAβ42 binding show 2- to 3-fold increases in remodeling activity (Fig. 4c, d), with an average remodeling activity of 83% compared to the NPT1098 scaffold.

To demonstrate that amyloid remodeling is a generic GAIM activity, we co-incubated tauKL fibers with GAIM fusions. TEM analysis of the complexes confirms that tauKL fibers lose their characteristic fibrillar conformation when co-incubated with GAIM fusions (Fig. 4e, f). Unlike fAβ42 fibers, tauKL fibers readily dissolve in low urea concentration solutions. To measure GAIM fusion-mediated ftauKL remodeling activity, we employed sarkosyl solubility assays. *In vitro* assembled tauKL fibers show resistance to dissolution when incubated with 1% sarkosyl. We subjected tauKL fibers treated with varying concentrations of GAIM fusions to 1% sarkosyl solution. Sarkosyl solubilized samples were then centrifuged at 100,000*g* to separate fibers from soluble tauKL. SDS-PAGE analysis for soluble tauKL shows that GAIM fusion-treated tauKL fibers dissolve in 1% sarkosyl, suggesting that these fibers can be remodeled in a concentration-dependent manner similarly to fAβ42 (Fig. 4g). Incubation with NPT1036, a super-stabilized GAIM fusion with no Aβ42 or tauKL fiber binding activity (Supplementary Fig. 3 and data not shown), shows no remodeling activity. Next, we compared remodeling efficiencies of NPT1098 with the two open-stabilized GAIM fusions, NPT1079 and NPT1087. Both NPT1079 and NPT1087 show enhanced remodeling activities, compared to NPT1098 (Fig. 4h).

Finally, we asked if remodeling of ftauKL results in release of soluble tauKL species. At the GAIM fusion concentrations for which we observe potent remodeling (EC_{50} = 10–250 nM), there are no soluble species seen in supernatants of complexes that have not been sarkosyl treated (Fig. 4g), suggesting that fiber remodeling by GAIM does not liberate soluble tauKL species.

Open-stabilized variants show increased assembly inhibition activity

We have previously reported the ability of GAIM fusions to protect neuronal cell lines from oligomer-induced toxicity in a concentration-dependent manner [15]. These experiments suggested that GAIM fusions can interact with intermediates formed during fiber assembly. To study the inhibitory effects of GAIM fusions on amyloid nucleation, we carried out Aβ42 assembly inhibition studies in the presence of varying concentrations of GAIM fusions. GAIM fusions potently block nucleation when present at sub-stoichiometric concentrations to Aβ42 monomers (Fig. 5a). The open-stabilized variants NPT1079 and NPT1087 show a dose-dependent increase in Aβ42 assembly inhibition potency. At 250 nM, NPT1079 and NPT1087 show a 20%–40% increase in inhibition potency compared to NPT1098 (Fig. 5a and b). The super-stabilized GAIM fusion NPT1036 showed no inhibitory effects on Aβ42 assembly (Fig. 5b).

Next, we studied the inhibitory effects of GAIM fusions on tauKL assembly. *In vitro* fiber assembly of full-length tau or truncated sequences, such as the microtubule-binding region, requires the presence of heparin to promote nucleation and subsequent assembly. GAIM fusions inhibited ftauKL assembly in the presence of heparin, and both NPT1079 and NPT1087 blocked nucleation 3- to 5-fold more effectively than NPT1098. Taken together, these results suggest that open conformation GAIM fusions bind both Aβ and tau on-pathway intermediates and inhibit amyloid assembly. It also shows that higher binding potency facilitates better inhibition of amyloid assembly.

Open-stabilized GAIM variants display potent binding to diverse amyloid fiber species and conformers

Studies aimed at identifying the pathological forms of Aβ in the AD-brain have shown that both insoluble plaque and soluble Aβ consists of a heterogeneous population of N- and C-terminal truncated Aβ peptides [10], forming structurally diverse conformations [7,28,29]. N-terminally truncated Aβ fragments might constitute the major part of the amyloid plaque [10]. To investigate whether the open-stabilized GAIM fusions are capable of engaging different conformations of Aβ aggregates, various modified Aβ peptides were fibrillized and binding affinities to these aggregates were measured. N-truncated Aβ11–42, Dutch mutation Aβ1–42 E22Q, and N-terminal pyro-glutamate modified Aβ11–42 and Aβ3–42 [30,31] were aggregated and fiber formation was verified by ThT and TEM (Supplementary Fig. 4). The aggregates formed using these peptides showed very diverse morphologies. For example, N-terminal pyro-glutamate-modified Aβ3–42 forms noodle-like fibers with several bends, Aβ1–42 E22Q forms smooth, long needle-like fibers and Aβ11–42 peptides form short, stubby fibers (Supplementary Fig. 4). Both the open variant NPT1079 and the original scaffold NPT1098 were found to engage the different fibers as measured by ELISA (Table 2 and Supplementary

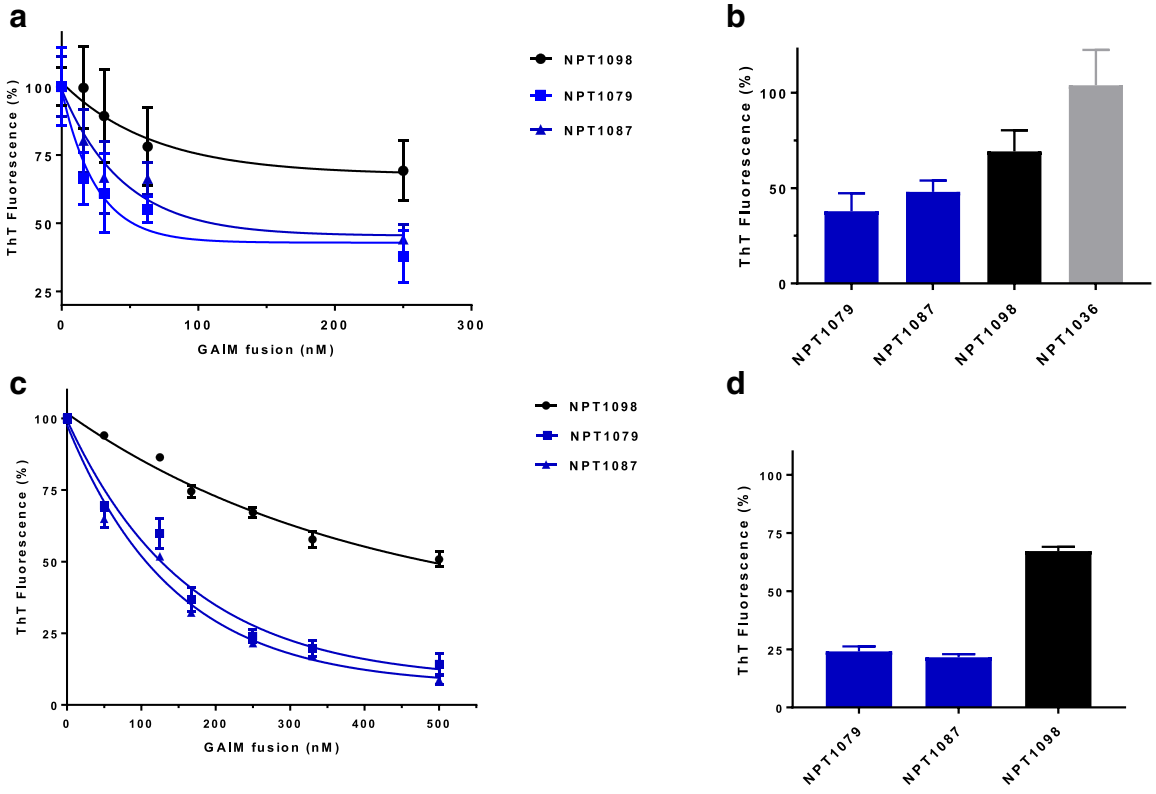

Fig. 5. Open-stable variants potently inhibit amyloid assembly. (a) Aβ42 fiber assembly is inhibited in a concentration-dependent manner by GAIM fusion. FAβ42 aggregation was measured by ThT fluorescence after 14-h incubation, and the percent ThT fluorescence was calculated with respect to fAb42 aggregation without GAIM fusion. (b) The open-stabilized GAIM fusions inhibit Aβ42 assembly more potently than NPT1098 at 250 nM GAIM fusion. NPT1036, a super-stabilized, disulfide-free GAIM with reduced infectivity (Kather *et al.*, [63]) and no binding activity to amyloids did not affect fiber assembly. (c) Concentration-dependent assembly inhibition of tauKL fiber by GAIM fusions. (d) Open-stabilized GAIM fusions show more potent assembly inhibition activity compared to NPT1098 at 250 nM of GAIM fusion. TauKL aggregation was measured by ThT fluorescence after 3 days of incubation, and percent aggregation was calculated relative tauKL aggregation without GAIM fusion. Error bars represent SD from three or more independent experiments.

Fig. 5). NPT1079 shows ~20-fold increased binding to the various aggregates (EC_{50} = 0.9–1.9 nM) compared to NPT1098. These data show that N-terminal truncations of Aβ do not affect GAIM fusion fiber binding, consistent with our previous NMR studies that show that GAIM engages the mid- and C-terminal sequences of Aβ42 fibers [14]. Studies on Aβ42 polymorphism suggest that the fibers assembled from these peptides are likely to contain different steric zippers, that is, a unique zipper for each proteoform [32]. GAIM fusions bind to several of these fibers with little difference in binding potencies, suggesting that there might be an inherent plasticity in the binding mechanism that allows these fusions to engage several aggregates.

Table 2. Open variant NPT1079 shows improved binding potency to multiple amyloid aggregates.

Binding target	NPT1098 EC_{50} (nM)	NPT1079 EC_{50} (nM)
Aβ1–42	18.0	0.8
Aβ11–42	24.3	0.9
Aβ3–42 pyroE3	24.1	1.1
Aβ11–42 pyroE11	40.6	1.9
Aβ1–42 E22Q	21.9	1.0
TolA-C	74.0	0.05
TauKL	59.0	14.0
CsgA	4.5	0.8
TTR (Wt)	105	7.0
Ig-V_L1C_L	25.0	24.0
Ig-V_L1	46.0	1.30
Ig-V_L2	13.0	19.0

Finally, we asked if these open-stabilized variants can target amyloid conformers associated with systemic amyloidosis [33–35]. Soluble TTR tetramer and three different immunoglobulin light-chain proteins, two Ig light-chain variable domain monomers (Ig-V_L1 and Ig-V_L2), and one Ig light-chain variable and constant domain dimer (Ig-V_L1C_L) were assembled into amyloids aggregates. The immunoglobulin domains carry mutations found in patients diagnosed with light-chain amyloidosis (see Supplementary Fig. 6). The open-

stabilized GAIM fusions bind these immunoglobulin light chain and TTR amyloids with low-nanomolar affinity (Table 2). Taken together, our data show that the open-stabilized GAIM fusions can bind a diverse array of amyloid aggregates in a conformation-dependent manner.

Discussion

To understand the structure–activity relationship of GAIM-amyloid interactions, we used site-directed mutagenesis to generate GAIM fusion variants. Characterization of these variants shows that binding potencies could be strengthened or weakened by over 250-fold for fAβ42 and over 100-fold for ftauKL (Fig. 2e), although no single mutation abolished binding to both amyloids. Furthermore, we show that mutations that reduced inter-domain interactions and expose the inner strands of the GAIM horseshoe (open conformers) improve amyloid binding (Fig. 2d). These variants contain amino acid changes either in the N1 domain (e.g., NPT189 [EC_{50} = 7.0 nM] and NPT1006 [EC_{50} = 2.4 nM]) or both the N1 and N2 domains (e.g., NPT1055 [EC_{50} = 0.7 nM] and NPT1077 [EC_{50} = 1.5 nM]). For all these variants, the Tm1, which reflects inter-domain separation and N2 unfolding, is decreased (Tables 1 and 3). While some of these mutations (T56H and R142I) are tolerated, others destabilize the domains dramatically, resulting in lower expression in HEK293 cells or increased non-specific binding to non-amyloid substrates (Supplementary Table 1).

Next, we explain the binding behavior of GAIM fusions carrying mutations in R142 located in the N2 domain and N39, T41, T51, and T56 located in N1 domain. These mutations alter amyloid binding by different mechanisms. Residue R142 is involved in several backbone and side-chain H-bonds (Fig. 6A). Replacing the charged R142 with large and non-polar residues such as isoleucine, phenylalanine, or histidine disrupts the H-bonding network in the N2 domain, leading to local instability in the N2 domain and reduced Tm1. This in turn exposes amyloid binding sites in the N1 domain.

Likewise, residues N39, T41, and T51 form extensive H-bonds with neighboring residues in the N1 domain. Replacing these residues with alanine or glycine residues does not perturb inter-domain interactions, seen by a minimal change in Tm1, but reduced amyloid binding (Supplementary Table 2). These results suggest that polar residues in β-strands 3, 4, and 5 influence binding by directly forming H-bonds with the amyloid aggregates. Replacing these polar residues with residues that do not participate in H-bonding results in variants that show differential loss in binding to amyloids. For example, N39A or T51G mutations show a 2-fold reduction in Aβ42 binding but a 10- to 180-fold reduction in tauKL binding.

Finally, GAIM fusion containing the polar mutation T56H shows both changes in Tm1 and differential binding to different amyloids. This GAIM variant, NPT189, is a marginally open conformer (Tm1 is 1.6 °C less that NPT1098 scaffold), and it shows a 4-fold increase in Aβ binding and a 2.5-fold improved binding to tauKL fibers, respectively. In addition, NPT189 shows an 8-fold increased binding to Aβ3–42 pyroE3 amyloid fibers and a 1400-fold increase in soluble TolA binding. While NPT189 shows altered binding for the aggregates mentioned above, it shows no change in binding to amyloid aggregates assembled from *E. coli* CsgA or from amyloid assembled from the immunoglobulin variable light chain.

Taken together, these results suggest that the mechanism of GAIM fusion binding to amyloid aggregates is strongly influenced by the H-bonding abilities of the polar residues in the N1 domain. Binding appears to be modulated by several physically separated clusters of amino acids, such as the N39 and T51 clusters, that are placed along the interdomain interface. The overall binding affinity to different amyloids depends on how many of these clusters are accessible to participate in H-bonding and how strongly they engage with the different types of amyloid aggregates.

Open conformers have two main structural differences from the NPT1098 scaffold. (1) They lack the interdomain interaction sequences in N1, which results in greater exposure of the amyloid binding sequences located in the vicinity of strands 4 and 5 in the N1 domain, and strands 9 and 10 in the N2 domain. (2) These variants also have more stabilized N2 domains. For example, the native N2

Table 3. Inter-domain interactions strongly influence amyloidβ binding.

Variant	Amino acid replacement (domain N1 or N1, N2)	Tm1 (°C)	Faβ42 EC_{50} (nM)	Additional comments
NPT1098	–	44.1	18	
NPT189	T56H (N1)	42.9	7.0	
NPT1006	T56H, T41W (N1)	42.1	2.4	
NPT1055	T56H, F190A, H191A (N1, N2)	39.0	0.7	Low yield, non-specific binding
NPT1009	T56H, QGGK (N1, N2)	47.7	356	
NPT1077	T56H, R142I (N1, N2)	41.6	1.5	

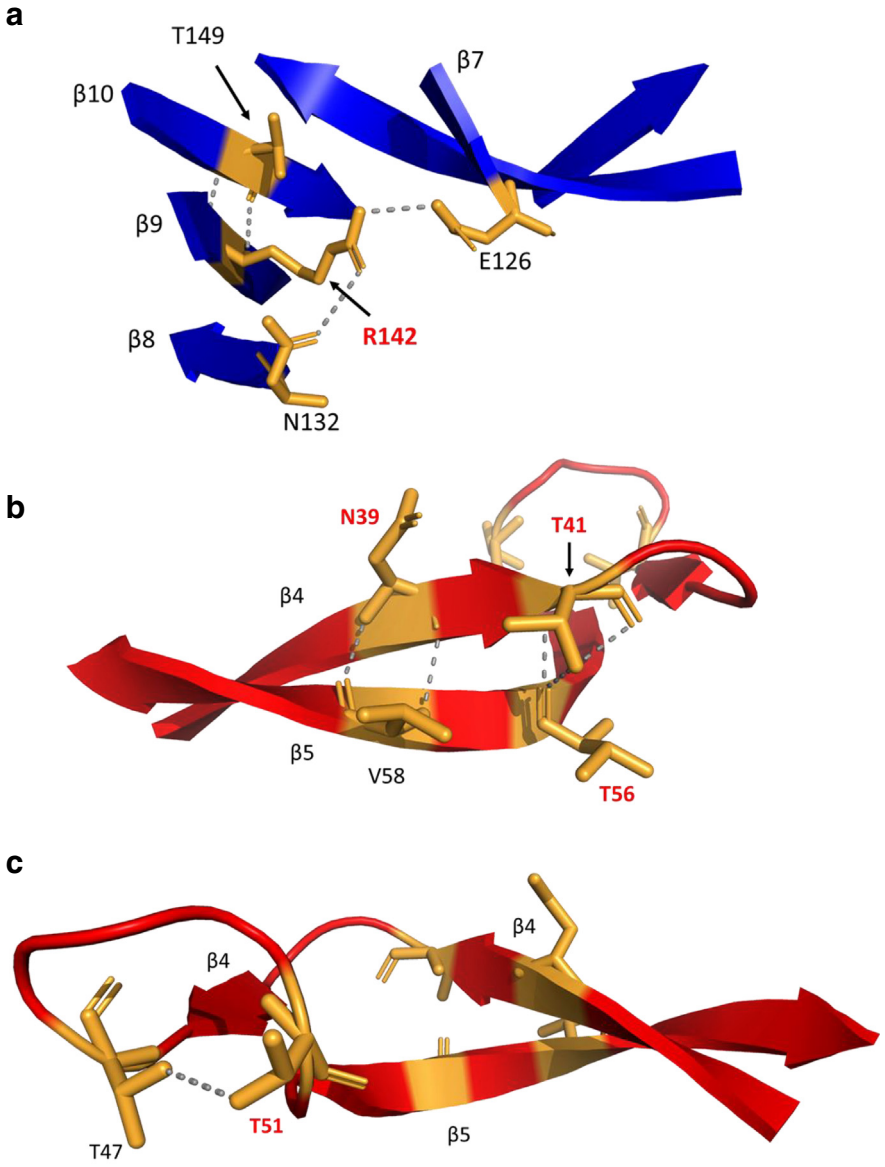

Fig. 6. Hydrogen bonding networks modulate amyloid binding. Ribbon diagrams showing hydrogen-bond networks in N2 domain in close proximity to residue R142 (A), N39, T41, and T56 (B) and residue T51. Bulky hydrophobic amino acid substitutions made at R142 break the H-bond networks and facilitate domain opening and target engagement. Alanine and glycine replacement in N1 polar residues inhibit amyloid binding without altering inter-domain interactions.

domain unfolds at 35 °C in the absence of the N1 domain [26] and the open variant NPT1079, with minimal N1 interactions, shows a Tm1 of 41.7 °C. We believe that the increased exposure of amyloid interacting residues and additional structural rearrangements of the topologically identical β-barrel domains (Supplementary Fig. 8) improves amyloid binding several fold. The improved plasticity could arise from stabilization of hydrophobic and aromatic binding clusters in the N2 domains. Further mutagenesis studies coupled with amyloid–GAIM hydrogen–deut exchange NMR experiments should allow us to map these binding sites in detail.

Amyloid assembly inhibition studies show that GAIM fusions can inhibit assembly at sub-stoichiometric concentrations. The GAIM fusion scaffold and the GAIM fusion variants with improved binding properties described in this study show no binding to unstructured or to structured soluble monomers. TTR is a tetramer (Supplementary Fig. 7). Thus, the mechanism of fiber assembly inhibition by GAIM is likely through GAIM binding at the growing end of either the early-stage assembly (e.g., oligomer) or the later-stage amyloid assembly (protofibrils or fibrils), preventing further monomer addition. The amyloid assembly inhibitory activity of

GAIM fusions is comparable to some other conformational binders previously described [36–40]. Similar to GAIM fusions, these molecules arrest amyloid assembly and their complexes with aggregates seed poorly and bind poorly to dyes like thioflavin T [37–39,41,42].

Solution-state NMR studies on g3pN1-TolA-C complexes show that N1 undergoes conformational rearrangement upon binding, seen as a major shift of the amide (NH) resonances in the N1 domain, as well as amide resonances outside the interacting interface [16,43]. This binding also alters the conformation of the TolA-C domain. Deprez *et al.* [43] have argued that this binding mechanism resembles an induced-fit model of substrate engagement as opposed to a lock and key model. In these studies, it was observed that structural plasticity in the N1 domain is essential to engage its target, TolA-C. Structural studies to gain insight into phage infection lend support to this unique model of binding. The TolA-C binding domains of closely related phages M13, IF1, and Ike unfold at 2.5, 3.9, and 5.4 M GdmCl, respectively, and their affinities for TolA-C correspondingly decrease in the same order at 0.4, 3.3, and 37.8 μM, respectively [27,44]. Mutations that restrict the domain flexibility of the M13 g3p, such as Q129H in the N2 domain and T13I in the N1 domain, dramatically reduce phage infection [17]. Our GAIM fusion binding studies also lend support to this mode of binding as GAIM fusions bind amyloid aggregates formed from diverse sequences (Aβ, tau, TTR, and LC) as well as different morphologies of Aβ aggregates (see Supplementary Fig. 4). An induced-fit mechanism of binding substrates, where GAIM progressively change conformation while engaging targets, could explain its capacity to engage diverse types of amyloid aggregates. Furthermore, NPT1015 (Q129H) and NPT1014 (T13I) reduced fAβ42 binding (by 7- and 25-fold, respectively), suggesting that N1 and N2 domain plasticity is important for binding to amyloids.

Remodeling studies show that sub-stoichiometric amounts of GAIM fusions bind to fAβ42 and alter the morphology of the fibers, and the altered amorphous conformer fails to bind ThT and has increased denaturant and detergent sensitivity. This remodeling activity seems to be both time- and concentration-dependent [14,15]. Open-stabilized GAIM fusion variants with increased amyloid binding activity also remodel fibers more effectively.

Based on these observations, amyloid remodeling can be explained in the following manner; Amyloid fibers in solution exist in a state of dynamic equilibrium with monomers and small oligomers that dissociate and re-associate to the ends of the fibers [45,46]. Furthermore, it is known that this dissociation of monomers and oligomers depends on the strength of the interactions between the monomers at the fiber ends and the number of exposed fiber ends. For example, Sanchez *et al.* [46] found that the dissociation of monomers from the Aβ40 fibers is 60 times faster than Aβ42 fibers. GAIM fusions are likely to alter this dynamic equilibrium by facilitating dissociation of monomers or oligomers from the fiber ends. The released species can then re-associate with free fiber ends, oligomerize and spontaneously nucleate into new seeds, or self-associate into non-fibrillar amorphous aggregates. Since GAIM fusions potently inhibit addition of monomers to fiber ends and block fresh nucleation, the released species are channeled to adopt non-fibrillar amorphous conformations. Although this passive mode of binding and remodeling has been suggested for several small molecules, such as epigallocatechin gallate, calmidazolium chloride, and dianilinophthalimide derivatives [47–51], GAIM fusions are likely to facilitate conversion of fibers into amorphous aggregates efficiently without releasing monomers or oligomers in solution.

Structural features unique to the GAIM scaffold likely to make remodeling more efficient include (1) the unusual binding and stability of the GAIM fusion-fiber complex. SPR studies show the off-rates of the open conformer NPT1079 ($K_d = 1.8 \times 10^{-5}$ 1/s) is about 15-fold slower than the N-terminal monoclonal antibody 6E10 ($K_d = 3.0 \times 10^{-4}$ 1/s). 6E10 does not remodel fibers in the same time frame as NPT1079. NPT1098, with a 5-fold faster off-rate compared to NPT1079 ($K_d = 9.5 \times 10^{-5}$ 1/s), produces partial remodeling (Supplementary Fig. 9). Thus, the overall binding affinity and stability of the complexes are likely to influence how many monomers or oligomers dissociate and what kind of amorphous aggregates the new associations subsequently form. (2) The induced-fit mechanism of GAIM binding to the central spine of amyloid fibers can perturb amyloid structure and facilitate faster dissociation. Similar alteration of the structure is seen when GAIM binds TolA-C, as described above [43]. (3) The GAIM scaffold contains 17 proline residues in the linker region (between the two domains and one proline in the N2 domain). Proline 213 in the linker region and Proline 161 in N2 are both known to undergo *cis–trans* isomerization. Amide exchange studies clearly show that proline isomerization is likely to induce large-scale conformational changes in the domains. For example, the *cis/trans* switching at P213 is propagated over an cα-cα distance between 13.7 (to G99) and 21.3 Å (Q206) [16]. Altering the orientation of the domains with respect to one another, when bound to fibers, is likely to induce structural changes in the fibers and alter their fibrillar morphology. Since the quaternary structures of the different amyloids are unlikely to be identical, the extent to which remodeling occurs and the nature of amorphous aggregates formed is likely to vary between amyloids. In fact, TEM images show some morphological differences between remodeled TauKL fibers and remodeled Aβ42 fibers (Fig. 4b and f). Further investigations of remodeling of different

amyloid species are required to understand this process.

Amyloid binding to GAIM parallels TolA-C interactions with its ligands: the phage tip protein g3p and group A colicins. Crystal structures of TolA-C complexed with the phage tip protein g3p or colicin A show a classic β-sheet augmentation; the interaction is mediated by a β-strand from one protein pairing with the edge strand in the binding domain of another protein to form a pseudo-continuous β sheet [27,52]. Both of these protein–protein interactions accommodate a large number of mutations without affecting their translocation across the bacterial membrane [53,54]. Backbone hydrogen bonds formed between the two interacting interfaces of g3p dictate the stability of the interactions [27,54]. Based on our studies on g3p and amyloid interactions, we believe that proteins binding to TolA and other promiscuous hub proteins [55] via β-strand/β-strand interactions can be engineered as ideal amyloid inhibitors and remodelers.

These studies might also help us understand certain aspects of phage–*E. coli* interactions and the necessity to recruit functional amyloids during certain stages of growth [56,57]. As phage infection is initiated by binding the promiscuous TolA protein, *E. coli* secretes a large amount of curli during stationary phase to sequester g3p and block phage infection. Preventing g3p binding would allow TolA to carry out other membrane-bound functions and cell-to-cell communication within the biofilms. *In vitro* binding studies show GAIM fusions bind CsgA fibers with high affinities (4.5 nM for NPT1098 and 0.78 nM for NPT1079).

We have shown that GAIM fusions interact broadly with multiple types of amyloid aggregates defined by different morphologies and aggregation properties, including those that are clinically relevant in neurodegenerative diseases, such as Alzheimer's disease and systemic protein misfolding disorders. GAIM fusions bind, inhibit assembly of, and convert insoluble amyloid fibers into non-fibrous amorphous aggregates. We believe that these binding and remodeling interactions could enhance opsonization and clearance by phagocytic cells. Taken together, our data presented here confirm and elaborate on earlier studies demonstrating that GAIM represents a unique mechanism for targeting a diverse array of amyloids implicated in protein misfolding diseases.

Materials and Methods

Generation of fusion proteins

GAIM–IgG fusion proteins were expressed using the Expi293 Expression System (Thermo Fisher Scientific) according to the manufacturer's instructions. Purification of the proteins was performed on HiTrap MabSelect SuRe column (GE Healthcare Life Sciences) in 20 mM sodium phosphate (pH 7.0), followed by a gradient elution in 20 mM sodium acetate from pH 4.0 to pH 3.6 over 20 CV using AKTA Pure FPLC system. IgG-fusion proteins were dialyzed into Dulbecco's phosphate-buffered saline (D-PBS; pH 7.4) and filter sterilized (Ultra-Free MC spin columns; Millipore). Protein purity was analyzed by NuPAGE 4%–12% Bis–Tris gel system with Mes SDS Running Buffer (Thermo Fisher Scientific) followed by InstantBlue Staining Solution (Expedeon). In addition, analytical SEC was used to assess the purity of Ig-fusions using a TSK gel G3000SW XL, 7.8 mm IDx30 cm, 5 μM column (Tosoh Bioscience) in an Ultimate 3000 UHPLC focused system (Thermo Fisher Scientific). For each sample, 7.5 μg of protein was injected onto the SEC column, and separation was performed in D-PBS mobile phase at a flow rate of 0.5 mL/min. Peak purity was analyzed using Chromeleon 7 software. GAIM–IgG fusion variants were synthesized by ATUM.

GdmCl-induced unfolding transitions

GAIM-dimer was separated from the IgG-fusions by specific cleavage in the Fc-linker by incubation with FabRICATOR (IdeS) enzyme (Genovis) for 3 h at 25 °C followed by separation from Fc by CaptoAdhere according to manufacturer's protocol. Purity of GAIM dimer was confirmed on NuPAGE 4%–12% Bis–Tris gel system separated in 2-(*N*-morpholino) ethanesulfonic acid (Mes) SDS Running Buffer. GAIM-dimer (0.5 μM) was incubated for 2 h at 25 °C in 100 mM potassium phosphate, pH 7.0 with increasing concentrations of GdmCl (Sigma). The fluorescence was measured in 10 mm cells at 310 and 340 nm after excitation at 280 nm, and at 360 nm after excitation at 295 nm. The data were analyzed using a two-state folding model assuming a linear dependence of fluorescence emissions on GdmCl concentration.

Aβ fiber assembly

Aβ1–42 (rPeptide), N-truncated Aβ11–42 (Bachem), Aβ11–42 Pyro (AnaSpec), Aβ3–42 Pyro (AnaSpec), and Aβ1–42 E22Q (AnaSpec) were dissolved in hexafluoroisopropanol and incubated at room temperature for 24 h until a clear solution developed. The peptide solution was dried under vacuum for 1 h. Fibers were assembled as described [58]. Aβ peptide (100 μg) was dissolved in 40 μL dimethyl sulfoxide, diluted in 1160 μL of 10 mM HCl solution and incubated with shaking at 500 rpm for 24 h at 37 °C. Fiber formation was confirmed by ThT.

TauKL expression, purification, and fiber assembly

Human tau fragment (tauKL) corresponding to residues 244–372 of Tau-441 (2N4R) with the P213L

mutation was expressed and purified as described for tau-MTBR [14]. TauKL fibers were assembled by adding 40 μM low-molecular-weight heparin (Fisher Scientific) to 40 μM tauKL monomer in 0.1 M sodium acetate (pH 7.0) buffer containing 2 mM DTT and incubated for 3 days at 37 °C. F*iber* formation was confirmed by ThT.

Transthyretin expression, purification, and aggregation

Expression and purification of recombinant TTR was carried out as described in [59,60] with minor changes. Competent *E. coli* (T7 express LysY) cells were transformed with pET11a vector containing the Human TTR (NM_000371.3) and grown in Terrific Broth medium supplemented with 100 mg/L ampicillin at 37 °C. Expression was induced with 1 mM IPTG when $OD_{600\ nm}$ = 0.6 and incubated for an additional 3.5 h at 30 °C, followed by centrifugation for 20 min at 10,000*g*. The pellet was re-suspended in lysis buffer [50 mM Tris–HCl (pH 8.0), 1 mg/mL lysozyme, 1 tab/10 mL cOmplete protease inhibitor cocktail containing EDTA, 5 mM DTT 125 KU/mL benzonase nuclease] and incubated on ice for 2 h, followed by sonication (10 s on, 10 s off) at amplitude 30 W for 5 min. Cell debris was removed from lysate by centrifugation at 200,000*g* for 30 min at 4 °C, followed by filtration through a 0.2-μm syringe filter. The protein was purified on an anion-exchange column (Resource Q, GE Healthcare) by a gradual increase in ionic strength. TTR fractions were pooled and further purified on a gel filtration column (Superdex75, GE Healthcare). Purified TTR was concentrated to >5 mg/mL ($\mathcal{E}$ = 77,600 M^{-1} cm^{-1} [61] in 50 mM sodium phosphate, 100 mM KCl, and 1 mM EDTA (pH 7.4) and stored at −80 °C. TTR was aggregated by diluting stock solution to a final concentration of 0.2 mg/mL in 50 mM sodium acetate (pH 4.0), 100 mM KCl, and 1 mM EDTA [60]. After 3 days at 37 °C, samples were thoroughly vortexed and analyzed by absorbance measurements at 400 nm via NanoDrop and ThT.

Recombinant immunoglobulin light-chain expression, purification, and aggregation

Light-chain sequences (Ig-V_L1, Ig-V_L2, and Ig-V_LC_L) carrying variable region mutations were obtained from the Boston School of Medicine Amyloidosis Center website (see Supplementary Fig. 6). Variable region sequences were cloned in the pD2610-v5 vector (ATUM Bio), with amino acids GGGGSEPEA added to the C-terminal of the sequences. The proteins were expressed in HEK293.2sus and purified by CaptureSelect C-tag Affinity Matrix (Thermo Fisher; cat no. 191307005) according to the manufacturer's protocol. Variable and constant domains sequences were cloned in the pD2610-v1 vector (ATUM). The protein was expressed in HEK293.2sus and purified by LambdaFab Select (GE; cat. no. 17548201) according to the manufacturer's protocol. Purified proteins were buffer exchanged into D-PBS, filter sterilized, and stored at −80 °C. Protein quality was examined by SDS-PAGE and HPLC-SEC. LC was aggregated by diluting stock solution to a final concentration of 0.05 mg/mL in 50 mM glycine/HCl (pH 3.0), 150 mM NaCl, 100 mM DTT, and 0.01% NaN_3. Samples were incubated at 37 °C for 7 days with rotation [62]. Fiber formation was confirmed by ThT.

Thermal unfolding of GAIM monitored by SO binding assay

GAIM–IgG fusion (1 μM) in phosphate-buffered saline (PBS) was mixed with 20× excess of SO (Invitrogen; cat. no. S-6650) in a 96-well plate and sealed. Thermal unfolding was monitored in a Roche LightCycler 480 RT-PCR by continuous increase in temperature from 20 °C to 95 °C at a rate of 0.24 °C/min. Excitation was set to 465 nm and emission to 580 nm with melt factor at 1, quant factor at 10, and maximum integration time for 2 s. The arbitrary unit of fluorescent signal was recorded and normalized to a scale of 0–100 [22].

Aβ and Tau binding ELISA

Fifty microliters of Aβ fiber (0.8 μM) or tauKL fiber (1 μM) in 50 mM carbonate buffer (pH 9.6) was added per well of a 96-well Maxisorp plate (Thermo Fisher) and incubated 16 h at 4 °C. Wells were washed with three times with D-PBS–Tween (0.05%) and two times with DPBS followed by blocking with SuperBlock (Thermo Scientific) for 1.5 h at room temperature. Wells were washed three times with PBS. GAIM–IgG fusion was added in high-concentration phosphate-buffered saline, 0.05% Tween 20 (PBS-T; 14.7 mM KH_2PO_4, 80.6 mM Na_2HPO_4–$7H_2O$, 27 mM KCl, 1.38 M NaCl, 0.05% Tween 20) at the indicated concentrations and incubated at 37 °C for 2 h, followed by three washes in D-PBS–Tween (0.05%) and three washes with DPBS. Human-specific Fc-HRP antibody (Jackson ImmunoResearch; cat. no. 109-035-008) was diluted 1:5000 in D-PBS–Tween (0.05%) containing 0.2% gelatin and incubated for 45 min at 37 °C. After two washes in D-PBS–Tween (0.05%) and two washes in DPBS, the signal was developed with TMB solution (Thermo Fisher), and the reaction was stopped by the addition of 0.25 N HCl. The absorbance at 450 nm was recorded with a Tecan Infinite M1000 PRO plate reader.

TolA binding ELISA

Fifty microliters of TolA (10 μM) in 14 mM sodium carbonate and 35 mM sodium bicarbonate (pH 9.6) diluted in distilled water and filtered through 0.22-μm

membrane was added to each well of a 96-well Maxisorp plate (Thermo Fisher) and incubated for 16 h at 4 °C. Wells were washed five times with D-PBS followed by blocking with SuperBlock (Thermo Scientific) for 2 h at 25 °C. Wells were washed five times with D-PBS–Tween (0.05%). GAIM–IgG fusion was added in D-PBS–Tween (0.05%) at the indicated concentrations and incubated at 37 °C for 1 h followed by five washes in D-PBS–Tween (0.05%). Human-specific Fc-HRP antibody (Jackson ImmunoResearch; cat. no. 109-035-008) was diluted 1:5000 in D-PBS–Tween (0.05%) containing 0.2% gelatin and added for 40 min at 37 °C. After three washes in D-PBS–Tween (0.05%) and four washes in DPBS, the signal was developed with TMB solution (Thermo Fisher), the reaction was stopped by the addition of 0.25 N HCl and the absorbance at 450 nm was recorded with a Tecan Infinite M1000 PRO plate reader.

TTR binding ELISA

Wells of a 96-well Maxisorp plate (Thermo Fisher) were blocked with 200 µL 1% bovine serum albumin (w/v) at 37 °C for 2 h. After three washes with DPBS, 50 µL 0.05 mg/mL TTR aggregates in aggregation buffer was added and the plate was incubated at 37 °C for 16 h. Wells were washed three times with distilled water and followed by one wash in D-PBS. GAIM fusion was added in high-concentration PBS-T (14.7 mM KH_2PO_4, 80.6 mM Na_2HPO_4–$7H_2O$, 27 mM KCl, 1.38 M NaCl, 0.05% Tween 20) at the indicated concentrations and incubated at 37 °C for 1 h followed by three washes in D-PBS–Tween (0.05%) and three washes in D-PBS. Human-specific Fc-HRP antibody (Jackson ImmunoResearch; cat. no. 109-035-008) diluted 1:5000 in D-PBS–Tween (0.05%) containing 0.2% gelatin was added for 40 min at 37 °C. After four washes in D-PBS–Tween (0.05%) and two washes in D-PBS, the signal was developed with TMB solution (Thermo Fisher). The reaction was stopped by the addition of 0.25 N HCl, and the absorbance at 450 nm was recorded with a Tecan Infinite M1000 PRO plate reader.

Ig-V_L1, Ig-V_L2, and Ig-V_LC_L binding ELISA

ELISA plates were prepared similar to TTR ELISA binding assay with minor changes; bovine serum albumin block was done at 37 °C for 3 h, and 50 µL of 0.025 mg/mL light-chain proteins was added to each well. GAIM–IgG fusion was diluted to 0–2.4 µM in high-concentration PBS-T (14.7 mM KH_2PO_4, 80.6 mM Na_2HPO_4–$7H_2O$, 27 mM KCl, 1.38 M NaCl, 0.05% Tween) and incubated at 37 °C for 80 min prior to being transferred to the plate with 50 µL sample in each well. After 2-h incubation at 37 °C, the plate was washed three times with D-PBS–Tween (0.05%) and three washes with DPBS. Human-specific Fc-HRP antibody (Jackson ImmunoResearch; cat. no. 109-035-008) diluted 1:5000 in D-PBS–Tween (0.05%) containing 0.2% gelatin was added for 45 min at 37 °C. After three washes in D-PBS–Tween (0.05%) and three washes in D-PBS, the signal was developed with TMB solution (Thermo Fisher), the reaction was stopped by the addition of 0.25 N HCl, and the absorbance at 450 nm was recorded with a Tecan Infinite M1000 PRO plate reader.

Non-specific binding ELISA

Four hundred fifty nanograms per well of human collagen (Sigma; cat. no. C5483) in D-PBS was immobilized on Medisorp 96-well plates (Thermo Fisher Scientific) for 16 h at 37 °C. Wells were washed three times with distilled water and one time with DPBS, followed by blocking in SuperBlock (Thermo Fisher Scientific) for 1 h at room temperature. GAIM–IgG fusion in D-PBS–Tween (0.05%) was incubated at 37 °C for 1 h 30 min, followed by three washes in D-PBS–Tween (0.05%) and three washes in D-PBS. Human-specific Fc-HRP antibody (Jackson ImmunoResearch; cat. no. 109-035-008) was added 1:5000 in PBS–Tween (0.05%) containing 0.2% gelatin and incubated for 45 min at 37 °C followed by four washes in PBS–Tween (0.05%) and two washes in PBS. The signal was developed with TMB solution (Sigma), and the reaction was stopped by the addition of 0.25 N HCl and the absorbance at 450 nm was recorded with a Tecan Infinite M1000 PRO plate reader.

Remodeling of Aβ42 fibers by GAIM–Ig fusion

Remodeling assays were carried out in low-retention microfuge tubes (Fisher Scientific; 02-681-320). All buffers contained 0.05% sodium azide to prevent microbial growth and total protein concentration in each sample after incubation was confirmed by reducing SDS-PAGE. Aβ42 fibers (2.5 µM) were co-incubated with or without GAIM–Ig fusion variants for 3 days at 37 °C. Aliquots of the complexes were then incubated with varying concentrations of urea. The ThT fluorescence of the complexes in urea was then plotted against the urea concentration. Remodeling efficiency at a fixed urea concentration was plotted as percent loss in ThT fluorescence compared to fibers without any GAIM–Ig fusion treatment.

Remodeling of tauKL fibers

Sarkosyl solubility assays were used to calculate the remodeling efficiencies of GAIM fusions. TauKL fibers (1 µM) were co-incubated with or without GAIM–Ig fusion variants at 37 °C for 5 days. Fibers and the complexes were incubated with or without 1% sarkosyl for 15 min and spun down at 100,000*g* for 30 min. The supernatant from each sample was carefully removed

and loaded on a 4%–12% NuPAGE gels (Invitrogen). Proteins were transferred to a nitrocellulose membrane and probed for tauKL. The percent remodeling was calculated by quantifying the gel bands using a Biorad Chemidoc system.

Aβ1–42 assembly inhibition assay

One hundred micrograms of hexafluoroisopropanol-treated Aβ1–42 (rPeptide) monomeric sample was dissolved in 80 μL dimethyl sulfoxide, mixed thoroughly by pipetting and vortexing, and diluted in 5.4 mL D-PBS to a final Aβ1–42 concentration of 4.04 μM. GAIM–IgG fusion samples were diluted in PBS to intermediate stock solutions of 10, 2.5, 0.63, and 0.16 μM. Eighty microliters of Aβ1–42 monomer solution was distributed in each well of a black, round bottom 96-well plate (LVL; cat. no. 225.LS.PP). Ten microliters of each stock solution of GAIM–IgG fusion samples was added to Aβ1–42 containing wells followed by the addition of 10 μL ThT (33 μM in D-PBS), for a final concentration of 3.2 μM Aβ1–42 and 3.3 μM ThT per well. The plate was sealed with transparent film, and ThT fluorescence at 430/485 nm (Ex/Em) was recorded every 20 min for 14 h in a Tecan Infinite M1000 PRO plate reader while incubated at 37 °C with 3 s of vertical shaking every 20 min. The percentage of Aβ42 aggregation for each NPT189 concentration was calculated relative to non-treated Aβ42 wells (positive control wells).

TauKL assembly inhibition assay

TauKL assembly reactions were set by incubating 10 μM monomers in 0.1 M sodium acetate (pH 7.0) buffer with 2 μM low-molecular-weight heparin (Fisher Scientific) at 37 °C for 3 days in the presence of varying concentrations of GAIM fusions (0–500 nM). ThT fluorescence of the assembly reactions was recorded by diluting samples to 1 μM in a 5 μM ThT solution. Inhibitory effects of GAIM on tauKL assembly were calculated by comparing the assembly of tauKL without any GAIM fusion.

TEM

Aβ1–42 fibers (15 μL of 20 μM sample) were applied on carbon-coated copper grids (Ted Pella; cat. no. 01844-F). Samples were then washed gently with 0.5 mL water, inverted, and floated over a drop of 2% uranyl acetate solution. After 30 s, the grids were removed and dried by wicking out the excess liquid from the edge of the grids using a filter paper. FEI technai spirit TEM was used to image the fibers. TauKL fibers (15 μL of 10 μM sample) were applied on carbon-coated copper grids (Ted Pella; cat. no. 01844-F) for 5 min. Samples were then washed gently with 0.5 mL water, followed by 7 drops of 2% uranyl acetate solution. The grids were immediately dried by wicking out the excess liquid from the edge of the grids using a filter paper. FEI technai spirit TEM was used to image the fibers.

CRediT authorship contribution statement

Eva Asp: Conceptualization, Supervision, Methodology, Investigation, Formal analysis, Writing - original draft, Writing - review & editing. **Ming Proschitsky:** Methodology, Investigation, Formal analysis, Writing - review & editing. **Michal Lulu:** Methodology, Investigation, Formal analysis, Writing - review & editing. **Cassandra Rockwell-Postel:** Methodology, Investigation, Formal analysis, Writing - review & editing. **Haim Tsubery:** Methodology, Investigation, Writing - review & editing. **Rajaraman Krishnan:** Conceptualization, Supervision, Methodology, Investigation, Formal analysis, Writing - original draft, Writing - review & editing.

Acknowledgments

We thank Dr. Richard Fisher and Dr. Jonathan M. Levenson at Proclara Biosciences for critical reading of the manuscript and valuable scientific discussions. We appreciate support in fusion protein purification process development and material from Jason Wright, at Proclara Biosciences.

Author Contributions: R.K., E.A., and H.T. conceived the project and planned the research. E.A., M.P., H.T., R.K., and M.L. designed mutants. M.L., M.P., C.R.P., and E.A. carried out the binding and protein unfolding studies. R.K., C.R.P., E.A., and M.P. carried out remodeling and TEM experiments. E.A. and R.K. analyzed the results and wrote the manuscript.

Appendix A. Supplementary data

Supplementary data to this article can be found online at https://doi.org/10.1016/j.jmb.2019.03.022.

Received 31 December 2018;
Received in revised form 19 March 2019;
Accepted 19 March 2019
Available online 28 March 2019

Keywords:
GAIM;
amyloid;
gene 3 protein;
SAR;

Abbreviations used:
D-PBS, Dulbecco's phosphate-buffered saline; GdmCl, guanidine hydrochloride; Mes, 2-(*N*-morpholino) ethanesulfonic acid; LC, immunoglobulin light chain; PBS-T, phosphate-buffered saline, 0.05% Tween 20; SEC, size-exclusion chromatography; SO, Sypro Orange; ThT, thioflavin T; TTR, transthyretin.

References

[1] R. Tycko, Physical and structural basis for polymorphism in amyloid fibrils, Protein Sci. 23 (2014) 1528–1539.
[2] R. Tycko, Amyloid polymorphism: structural basis and neurobiological relevance, Neuron 86 (2015) 632–645.
[3] J.C. Watts, C. Condello, J. Stohr, A. Oehler, J. Lee, S.J. DeArmond, L. Lannfelt, M. Ingelsson, K. Giles, S.B. Prusiner, Serial propagation of distinct strains of Abeta prions from Alzheimer's disease patients, Proc. Natl. Acad. Sci. U. S. A. 111 (2014) 10323–10328.
[4] A.L. Woerman, A. Aoyagi, S. Patel, S.A. Kazmi, I. Lobach, L.T. Grinberg, A.C. McKee, W.W. Seeley, S.H. Olson, S.B. Prusiner, Tau prions from Alzheimer's disease and chronic traumatic encephalopathy patients propagate in cultured cells, Proc. Natl. Acad. Sci. U. S. A. 113 (2016) E8187–E8196.
[5] J.C. Watts, S.B. Prusiner, Beta-amyloid prions and the pathobiology of Alzheimer's disease, Cold Spring Harb. Perspect. Med. 8 (2018).
[6] S.K. Kaufman, T.L. Thomas, K. Del Tredici, H. Braak, M.I. Diamond, Characterization of tau prion seeding activity and strains from formaldehyde-fixed tissue, Acta Neuropathol. Commun. 5 (2017) 41.
[7] C. Condello, T. Lemmin, J. Stohr, M. Nick, Y. Wu, A.M. Maxwell, J.C. Watts, C.D. Caro, A. Oehler, C.D. Keene, T.D. Bird, S.G. van Duinen, L. Lannfelt, M. Ingelsson, C. Graff, K. Giles, W.F. DeGrado, S.B. Prusiner, Structural heterogeneity and intersubject variability of Abeta in familial and sporadic Alzheimer's disease, Proc. Natl. Acad. Sci. U. S. A. 115 (2018) E782–E791.
[8] W. Qiang, W.M. Yau, J.X. Lu, J. Collinge, R. Tycko, Structural variation in amyloid-beta fibrils from Alzheimer's disease clinical subtypes, Nature 541 (2017) 217–221.
[9] A.W.P. Fitzpatrick, B. Falcon, S. He, A.G. Murzin, G. Murshudov, H.J. Garringer, R.A. Crowther, B. Ghetti, M. Goedert, S.H.W. Scheres, Cryo-EM structures of tau filaments from Alzheimer's disease, Nature 547 (2017) 185–190.
[10] N.C. Wildburger, T.J. Esparza, R.D. LeDuc, R.T. Fellers, P.M. Thomas, N.J. Cairns, N.L. Kelleher, R.J. Bateman, D.L. Brody, Diversity of amyloid-beta proteoforms in the Alzheimer's disease brain, Sci. Rep. 7 (2017) 9520.
[11] C. Sato, N.R. Barthelemy, K.G. Mawuenyega, B.W. Patterson, B.A. Gordon, J. Jockel-Balsarotti, M. Sullivan, M.J. Crisp, T. Kasten, K.M. Kirmess, N.M. Kanaan, K.E. Yarasheski, A. Baker-Nigh, T.L.S. Benzinger, T.M. Miller, C. M. Karch, R.J. Bateman, Tau kinetics in neurons and the human central nervous system, Neuron 98 (2018) 861–864.
[12] N. Sergeant, S. Bombois, A. Ghestem, H. Drobecq, V. Kostanjevecki, C. Missiaen, A. Wattez, J.P. David, E. Vanmechelen, C. Sergheraert, A. Delacourte, Truncated beta-amyloid peptide species in pre-clinical Alzheimer's disease as new targets for the vaccination approach, J. Neurochem. 85 (2003) 1581–1591.
[13] J. Naslund, A. Schierhorn, U. Hellman, L. Lannfelt, A.D. Roses, L.O. Tjernberg, J. Silberring, S.E. Gandy, B. Winblad, P. Greengard, et al., Relative abundance of Alzheimer a beta amyloid peptide variants in Alzheimer disease and normal aging, Proc. Natl. Acad. Sci. U. S. A. 91 (1994) 8378–8382.
[14] R. Krishnan, H. Tsubery, M.Y. Proschitsky, E. Asp, M. Lulu, S. Gilead, M. Gartner, J.P. Waltho, P.J. Davis, A.M. Hounslow, D.A. Kirschner, H. Inouye, D.G. Myszka, J. Wright, B. Solomon, R.A. Fisher, A bacteriophage capsid protein provides a general amyloid interaction motif (GAIM) that binds and remodels misfolded protein assemblies, J. Mol. Biol. 426 (2014) 2500–2519.
[15] J.M. Levenson, S. Schroeter, J.C. Carroll, V. Cullen, E. Asp, M. Proschitsky, C.H. Chung, S. Gilead, M. Nadeem, H.B. Dodiya, S. Shoaga, E.J. Mufson, H. Tsubery, R. Krishnan, J. Wright, B. Solomon, R. Fisher, K.S. Gannon, NPT088 reduces both amyloid-beta and tau pathologies in transgenic mice, Alzheimers Dement. (N Y) 2 (2016) 141–155.
[16] U. Weininger, R.P. Jakob, B. Eckert, K. Schweimer, F.X. Schmid, J. Balbach, A remote prolyl isomerization controls domain assembly via a hydrogen bonding network, Proc. Natl. Acad. Sci. U. S. A. 106 (2009) 12335–12340.
[17] A. Martin, F.X. Schmid, A proline switch controls folding and domain interactions in the gene-3-protein of the filamentous phage fd, J. Mol. Biol. 331 (2003) 1131–1140.
[18] B. Eckert, F.X. Schmid, A conformational unfolding reaction activates phage fd for the infection of *Escherichia coli*, J. Mol. Biol. 373 (2007) 452–461.
[19] A. Martin, F.X. Schmid, Evolutionary stabilization of the gene-3-protein of phage fd reveals the principles that govern the thermodynamic stability of two-domain proteins, J. Mol. Biol. 328 (2003) 863–875.
[20] S. Hoffmann-Thoms, U. Weininger, B. Eckert, R.P. Jakob, J.R. Koch, J. Balbach, F.X. Schmid, Initiation of phage infection by partial unfolding and prolyl isomerization, J. Biol. Chem. 288 (2013) 12979–12991.
[21] L.W. Deng, R.N. Perham, Delineating the site of interaction on the pIII protein of filamentous bacteriophage fd with the F-pilus of *Escherichia coli*, J. Mol. Biol. 319 (2002) 603–614.
[22] C.J. Layton, H.W. Hellinga, Quantitation of protein–protein interactions by thermal stability shift analysis, Protein Sci. 20 (2011) 1439–1450.
[23] M.W. Traxlmayr, M. Faissner, G. Stadlmayr, C. Hasenhindl, B. Antes, F. Ruker, C. Obinger, Directed evolution of stabilized IgG1-Fc scaffolds by application of strong heat shock to libraries displayed on yeast, Biochim. Biophys. Acta 1824 (2012) 542–549.
[24] P. Holliger, L. Riechmann, R.L. Williams, Crystal structure of the two N-terminal domains of g3p from filamentous phage fd at 1.9 Å: evidence for conformational lability, J. Mol. Biol. 288 (1999) 649–657.
[25] R.P. Jakob, B.K. Zierer, U. Weininger, S.D. Hofmann, S.H. Lorenz, J. Balbach, H. Dobbek, F.X. Schmid, Elimination of a cis-proline-containing loop and turn optimization stabilizes a protein and accelerates its folding, J. Mol. Biol. 399 (2010) 331–346.
[26] S. Hoffmann-Thoms, R.P. Jakob, F.X. Schmid, Energetic communication between functional sites of the gene-3-protein during infection by phage fd, J. Mol. Biol. 426 (2014) 1711–1722.
[27] S.H. Lorenz, R.P. Jakob, U. Weininger, J. Balbach, H. Dobbek, F.X. Schmid, The filamentous phages fd and IF1 use different mechanisms to infect *Escherichia coli*, J. Mol. Biol. 405 (2011) 989–1003.

[28] J. Rasmussen, J. Mahler, N. Beschorner, S.A. Kaeser, L.M. Hasler, F. Baumann, S. Nystrom, E. Portelius, K. Blennow, T. Lashley, N.C. Fox, D. Sepulveda-Falla, M. Glatzel, A.L. Oblak, B. Ghetti, K.P.R. Nilsson, P. Hammarstrom, M. Staufenbiel, L.C. Walker, M. Jucker, Amyloid polymorphisms constitute distinct clouds of conformational variants in different etiological subtypes of Alzheimer's disease, Proc. Natl. Acad. Sci. U. S. A. 114 (2017) 13018–13023.

[29] J. Liu, I. Costantino, N. Venugopalan, R.F. Fischetti, B.T. Hyman, M.P. Frosch, T. Gomez-Isla, L. Makowski, Amyloid structure exhibits polymorphism on multiple length scales in human brain tissue, Sci. Rep. 6 (2016), 33079.

[30] E. Levy, M.D. Carman, I.J. Fernandez-Madrid, M.D. Power, I. Lieberburg, S.G. van Duinen, G.T. Bots, W. Luyendijk, B. Frangione, Mutation of the Alzheimer's disease amyloid gene in hereditary cerebral hemorrhage, Dutch type, Science 248 (1990) 1124–1126.

[31] C. Van Broeckhoven, J. Haan, E. Bakker, J.A. Hardy, W. Van Hul, A. Wehnert, M. Vegter-Van der Vlis, R.A. Roos, Amyloid beta protein precursor gene and hereditary cerebral hemorrhage with amyloidosis (Dutch), Science 248 (1990) 1120–1122.

[32] J.P. Colletier, A. Laganowsky, M. Landau, M. Zhao, A.B. Soriaga, L. Goldschmidt, D. Flot, D. Cascio, M.R. Sawaya, D. Eisenberg, Molecular basis for amyloid-beta polymorphism, Proc. Natl. Acad. Sci. U. S. A. 108 (2011) 16938–16943.

[33] G. Merlini, V. Bellotti, Molecular mechanisms of amyloidosis, N. Engl. J. Med. 349 (2003) 583–596.

[34] M.A. Gertz, M.D. Benson, P.J. Dyck, M. Grogan, T. Coelho, M. Cruz, J.L. Berk, V. Plante-Bordeneuve, H.H.J. Schmidt, G. Merlini, Diagnosis, prognosis, and therapy of transthyretin amyloidosis, J. Am. Coll. Cardiol. 66 (2015) 2451–2466.

[35] M.A. Gertz, Immunoglobulin light chain amyloidosis diagnosis and treatment algorithm 2018, Blood Cancer J. 8 (2018) 44.

[36] B. O'Nuallain, R. Wetzel, Conformational Abs recognizing a generic amyloid fibril epitope, Proc. Natl. Acad. Sci. U. S. A. 99 (2002) 1485–1490.

[37] G. Habicht, C. Haupt, R.P. Friedrich, P. Hortschansky, C. Sachse, J. Meinhardt, K. Wieligmann, G.P. Gellermann, M. Brodhun, J. Gotz, K.J. Halbhuber, C. Rocken, U. Horn, M. Fandrich, Directed selection of a conformational antibody domain that prevents mature amyloid fibril formation by stabilizing Abeta protofibrils, Proc. Natl. Acad. Sci. U. S. A. 104 (2007) 19232–19237.

[38] I. Morgado, K. Wieligmann, M. Bereza, R. Ronicke, K. Meinhardt, K. Annamalai, M. Baumann, J. Wacker, P. Hortschansky, M. Malesevic, C. Parthier, C. Mawrin, C. Schiene-Fischer, K.G. Reymann, M.T. Stubbs, J. Balbach, M. Gorlach, U. Horn, M. Fandrich, Molecular basis of beta-amyloid oligomer recognition with a conformational antibody fragment, Proc. Natl. Acad. Sci. U. S. A. 109 (2012) 12503–12508.

[39] A.R. Ladiwala, M. Bhattacharya, J.M. Perchiacca, P. Cao, D.P. Raleigh, A. Abedini, A.M. Schmidt, J. Varkey, R. Langen, P.M. Tessier, Rational design of potent domain antibody inhibitors of amyloid fibril assembly, Proc. Natl. Acad. Sci. U. S. A. 109 (2012) 19965–19970.

[40] R. Kayed, E. Head, J.L. Thompson, T.M. McIntire, S.C. Milton, C.W. Cotman, C.G. Glabe, Common structure of soluble amyloid oligomers implies common mechanism of pathogenesis, Science 300 (2003) 486–489.

[41] C.S. Gruning, S. Klinker, M. Wolff, M. Schneider, K. Toksoz, A.N. Klein, L. Nagel-Steger, D. Willbold, W. Hoyer, The off-rate of monomers dissociating from amyloid-beta protofibrils, J. Biol. Chem. 288 (2013) 37104–37111.

[42] R. Krishnan, J.L. Goodman, S. Mukhopadhyay, C.D. Pacheco, E.A. Lemke, A.A. Deniz, S. Lindquist, Conserved features of intermediates in amyloid assembly determine their benign or toxic states, Proc. Natl. Acad. Sci. U. S. A. 109 (2012) 11172–11177.

[43] C. Deprez, R. Lloubes, M. Gavioli, D. Marion, F. Guerlesquin, L. Blanchard, Solution structure of the *E. coli* TolA C-terminal domain reveals conformational changes upon binding to the phage g3p N-terminal domain, J. Mol. Biol. 346 (2005) 1047–1057.

[44] R.P. Jakob, A.J. Geitner, U. Weininger, J. Balbach, H. Dobbek, F.X. Schmid, Structural and energetic basis of infection by the filamentous bacteriophage IKe, Mol. Microbiol. 84 (2012) 1124–1138.

[45] N. Carulla, G.L. Caddy, D.R. Hall, J. Zurdo, M. Gairi, M. Feliz, E. Giralt, C.V. Robinson, C.M. Dobson, Molecular recycling within amyloid fibrils, Nature 436 (2005) 554–558.

[46] L. Sanchez, S. Madurga, T. Pukala, M. Vilaseca, C. Lopez-Iglesias, C.V. Robinson, E. Giralt, N. Carulla, Abeta40 and Abeta42 amyloid fibrils exhibit distinct molecular recycling properties, J. Am. Chem. Soc. 133 (2011) 6505–6508.

[47] J. Bieschke, J. Russ, R.P. Friedrich, D.E. Ehrnhoefer, H. Wobst, K. Neugebauer, E.E. Wanker, EGCG remodels mature alpha-synuclein and amyloid-beta fibrils and reduces cellular toxicity, Proc. Natl. Acad. Sci. U. S. A. 107 (2010) 7710–7715.

[48] B.E. Roberts, M.L. Duennwald, H. Wang, C. Chung, N.P. Lopreiato, E.A. Sweeny, M.N. Knight, J. Shorter, A synergistic small-molecule combination directly eradicates diverse prion strain structures, Nat. Chem. Biol. 5 (2009) 936–946.

[49] J.D. Harper, S.S. Wong, C.M. Lieber, P.T. Lansbury, Observation of metastable Abeta amyloid protofibrils by atomic force microscopy, Chem. Biol. 4 (1997) 119–125.

[50] A.D. Williams, M. Sega, M. Chen, I. Kheterpal, M. Geva, V. Berthelier, D.T. Kaleta, K.D. Cook, R. Wetzel, Structural properties of Abeta protofibrils stabilized by a small molecule, Proc. Natl. Acad. Sci. U. S. A. 102 (2005) 7115–7120.

[51] H. Wang, M.L. Duennwald, B.E. Roberts, L.M. Rozeboom, Y.L. Zhang, A.D. Steele, R. Krishnan, L.J. Su, D. Griffin, S. Mukhopadhyay, E.J. Hennessy, P. Weigele, B.J. Blanchard, J. King, A.A. Deniz, S.L. Buchwald, V.M. Ingram, S. Lindquist, J. Shorter, Direct and selective elimination of specific prions and amyloids by 4,5-dianilinophthalimide and analogs, Proc. Natl. Acad. Sci. U. S. A. 105 (2008) 7159–7164.

[52] P. Holliger, L. Riechmann, A conserved infection pathway for filamentous bacteriophages is suggested by the structure of the membrane penetration domain of the minor coat protein g3p from phage fd, Structure 5 (1997) 265–275.

[53] F. Karlsson, A.C. Malmborg-Hager, C.A. Borrebaeck, *Escherichia coli* TolA tolerates multiple amino-acid substitutions as revealed by screening randomized variants for membrane integrity and phage receptor function, FEMS Microbiol. Lett. 259 (2006) 81–88.

[54] C. Li, Y. Zhang, M. Vankemmelbeke, O. Hecht, F.S. Aleanizy, C. Macdonald, G.R. Moore, R. James, C.N. Penfold, Structural evidence that colicin A protein binds to a novel binding site of TolA protein in *Escherichia coli* periplasm, J. Biol. Chem. 287 (2012) 19048–19057.

[55] A. Patil, K. Kinoshita, H. Nakamura, Hub promiscuity in protein–protein interaction networks, Int. J. Mol. Sci. 11 (2010) 1930–1943.

[56] J.E. Price, M.R. Chapman, Phaged and confused by biofilm matrix, Nat. Microbiol. 3 (2018) 2–3.

[57] L. Vidakovic, P.K. Singh, R. Hartmann, C.D. Nadell, K. Drescher, Dynamic biofilm architecture confers individual and collective mechanisms of viral protection, Nat. Microbiol. 3 (2018) 26–31.
[58] W.B. Stine Jr., K.N. Dahlgren, G.A. Krafft, M.J. LaDu, In vitro characterization of conditions for amyloid-beta peptide oligomerization and fibrillogenesis, J. Biol. Chem. 278 (2003) 11612–11622.
[59] K. Andersson, M. Pokrzywa, I. Dacklin, E. Lundgren, Inhibition of TTR aggregation-induced cell death—a new role for serum amyloid P component, PLoS One 8 (2013), e55766.
[60] E. Lundberg, A. Olofsson, G.T. Westermark, A.E. Sauer-Eriksson, Stability and fibril formation properties of human and fish transthyretin, and of the *Escherichia coli* transthyretin-related protein, FEBS J. 276 (2009) 1999–2011.
[61] P. Mangrolia, D.T. Yang, R.M. Murphy, Transthyretin variants with improved inhibition of beta-amyloid aggregation, Protein Eng. Des. Sel. 29 (2016) 209–218.
[62] K. Andrich, U. Hegenbart, C. Kimmich, N. Kedia, H.R. Bergen 3rd, S. Schonland, E. Wanker, J. Bieschke, Aggregation of full-length immunoglobulin light chains from systemic light chain amyloidosis (AL) patients is remodeled by epigallocatechin-3-gallate, J. Biol. Chem. 292 (2017) 2328–2344.
[63] I. Kather, C.A Bippes, F.X. Schmid, A stable disulfide-free gene-3-protein of phage fd generated by in vitro evolution, J Mol Biol. 354 (3) (2005) 666–678.